Journal Pre-proof

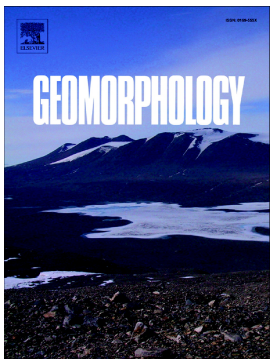

Reconstructing the Chongbaxia Tsho glacial lake outburst flood in the Eastern Himalaya: Evolution, process and impacts

Yong Nie, Wei Liu, Qiao Liu, Xu Hu, Matthew J. Westoby

PII: S0169-555X(20)30366-4

DOI: https://doi.org/10.1016/j.geomorph.2020.107393

Reference: GEOMOR 107393

To appear in: *Geomorphology*

Received date: 9 January 2020

Revised date: 11 August 2020

Accepted date: 18 August 2020

Please cite this article as: Y. Nie, W. Liu, Q. Liu, et al., Reconstructing the Chongbaxia Tsho glacial lake outburst flood in the Eastern Himalaya: Evolution, process and impacts, *Geomorphology* (2018), https://doi.org/10.1016/j.geomorph.2020.107393

Reconstructing the Chongbaxia Tsho glacial lake outburst flood in the Eastern Himalaya: evolution, process and impacts

Yong Nie[1, 2, *], Wei Liu[1], Qiao Liu[1, 2], Xu Hu[1], Matthew J Westoby[3]

[1]Institute of Mountain Hazards and Environment, Chinese Academy of Sciences, Chengdu, Sichuan 610041, China

[2]University of Chinese Academy of Sciences, Beijing 100190, China

[3]Department of Geography and Environmental Sciences, Northumbria University, Newcastle upon Tyne, United Kingdom

*Corresponding author: Yong Nie

E-mail: nieyong@imde.ac.cn

Abstract: Glacial lake outburst floods (GLOF) are one of the most destructive natural disasters. Understanding GLOF evolution, and their impacts, plays a fundamental role in GLOF hazard assessment and risk management. Reconstructing historical GLOFs is an important exercise because detailed case studies of such glacial hazards are rare, which hinders the capacity of glacial hazard practitioners to learn from these events. In this study, we reconstruct a historical GLOF from moraine-dammed Chongbaxia Tsho (89.745°E, 28.211°N) in the Eastern Himalaya, which is a unique case study because the outburst flood cascaded into two further lakes downstream. We employ a combination of i) multi-source and multi-temporal satellite imagery, ii) field investigation (including an unmanned aerial vehicle survey), iii) numerical dam breach and hydrodynamic modelling and, iv) qualitative and quantitative cryospheric and meteorological analysis to investigate the evolution of the GLOF hazard, simulate moraine dam failure and GLOF propagation, and explore the role that long- and short-term climate trends played in providing the conditioning factors for the outburst. Chongbaxia Tsho expanded rapidly between 1987 until 2001 in response to glacier recession most likely caused by a regional warming trend of +0.37°C per decade. Based on satellite image analysis we refine the outburst date to be 6 August 2001, instead of 6 August, 2000, as previously believed, and attribute an ice avalanche into the glacial lake originating from the receding parent glacier as the most likely trigger for moraine dam failure. Through DEM differencing and lake level decrease, we estimate that a total water volume of 27.1±1.6 × 10^6 m^3 was released from the lake during the event, and using dam breach modelling we estimate that the peak discharge at the breach was >6600 m^3 s^{-1}. The GLOF flowed through downstream Chongbamang Tsho and Chongbayong Tsho, both of which served to attenuate the GLOF and reduce downstream losses; the latter stored an estimated 96% of the flood volume. Precipitation totals in the weeks preceding the GLOF exceeded the historical mean by up to 40%, and may have contributed to instability of the parent glacier, and generation of an ice avalanche with enough impact energy to cause lake water to overtop the moraine dam

and initiate breach development. A future GLOF from Chongbaxia Tsho cannot be ruled out, but more field data, including detailed lake bathymetry, and information pertaining to the sedimentological and geotechnical characteristics of the moraine dam, are required for a more robust parameterization of a predictive GLOF model and quantification of the hazard posed by a future GLOF.

Key words: GLOFs; climate change; glaciers; Himalayas; remote sensing

1. Introduction

The Himalaya, including the Tibetan Plateau, hosts the largest volume of glacier ice outside of the polar regions (Farinotti et al., 2019) and is commonly referred to as the 'Asian water tower' (Immerzeel et al., 2010; Yao et al., 2012). Glaciers across the Tibetan Plateau sustain river flows outside of periods of high seasonal precipitation, play an important role in provisioning water for use as a drinking supply and for industry, and are an important tourism and cultural asset (Immerzeel et al., 2010; Wang et al., 2019). However, the region is characterized by glacial retreat and negative mass balance (Nie et al., 2010; Yao et al., 2012; Gao et al., 2019; Wang et al., 2019), and the rate of ice loss has accelerated in past decades (Maurer et al., 2019). As well as directly impacting the water resource for downstream communities (Immerzeel et al., 2010; Biemans et al., 2019), climate-driven cryospheric change also has implications for the evolution of glacier-related hazards (Yao et al., 2012; Immerzeel et al., 2013), including glacial lake outburst floods (GLOFs) (Huss et al., 2017; Harrison et al., 2018).

The frequency of Himalayan GLOFs make this region one of the world's most vulnerable zones for this phenomena (Quincey et al., 2005; Carrivick and Tweed, 2016; Stoffel et al., 2016; Nie et al., 2017; Rounce et al., 2017; Nie et al., 2018; Allen et al., 2019; Byers et al., 2019; Veh et al., 2019). The outbursts of Cirenmaco within Tibet, China, in 1981 (Xu and Feng, 1989; Chen et al., 2007; ICIMOD (The International Centre for Integrated Mountain Development), 2011) and Chorabari Lake in 2013 killed hundreds of people (Allen et al., 2016), whilst many hydropower plants have also been severely damaged or destroyed

by GLOFs across the region (Mool et al., 2001; ICIMOD, 2011) with resulting economic losses totaling millions of US dollars. Hundreds of Himalayan hydropower projects (Zarfl et al., 2015; Schwanghart et al., 2016) are proposed or are currently under construction to exploit the considerable hydroelectricity potential of the region and to meet the soaring energy demand in South Asia (Hennig, 2015; BP, 2019), however, most of these sites are located in glacierized watersheds and are potentially threatened by GLOFs. Hazard and risk assessment of future GLOFs is necessary to identify options for mitigating potential GLOF impacts, an exercise which is becoming increasingly important as glacial lakes expand in response to climate change (Nie et al., 2017) and the frequency of key trigger mechanisms, such as ice and rock avalanches and glacier ice detachments, is predicted to become more frequent (Haeberli, 2017). However, despite a growing body of GLOF-related literature, detailed case studies of historical GLOFs, and most notably those involving multiple lake cascades, are rare, yet knowledge gained from these events can be used to inform future hazard assessment strategies. By reconstructing past events we can gain knowledge and insight into key processes and mechanisms in the GLOF process-chain (Mergili et al., 2018), and assess the accuracy of hazard and risk appraisals (Nie et al., 2018).

Current databases of Himalayan GLOF events have been compiled using field surveys, remote sensing observation and literature searches (Nie et al., 2018; Byers et al., 2019; Veh et al., 2019) and have improved our understanding of GLOF magnitude, frequency, and trigger mechanisms. Most Himalayan GLOFs are the result of moraine dam failures that have been initiated by overtopping or piping (Westoby et al., 2014a), the former of which is commonly

triggered by ice, rock or snow avalanching, glacier calving, short-lived extreme precipitation (Allen et al., 2016), earthquake and ice-cored moraine degradation (Richardson and Reynolds, 2000; ICIMOD, 2011; Westoby et al., 2014a; Allen et al., 2016; Stoffel et al., 2016; Byers et al., 2019). Most Himalayan glacial lakes are located in high-altitude areas (>4000 m above sea level) (Nie et al., 2017) and low accessibility makes the field investigation of glacial lakes, which is important for in situ evaluation and validation of glacial lake and GLOF attributes, difficult. Hence, some key attributes of newly discovered GLOFs, including event date, likely triggers, and downstream impacts, are unclear. This is the case for Chongbaxia Tsho in the Eastern Himalaya, which is the focus of this study (**Fig. 1**).

Remote sensing is widely regarded as a highly feasible technique for detecting historical GLOFs, monitoring the past and current status of glacial lakes, and predicting their future evolution (Quincey et al., 2005; Nie et al., 2017; Rounce et al., 2017; Sattar et al., 2019; Veh et al., 2019). More recently, imagery acquired from Unmanned Aerial Vehicles (UAV) and processed using digital photogrammetric reconstruction has been used to generate high spatial resolution orthomosaics and digital elevation models (DEM) which with to investigate moraine-dammed lake catchments and GLOF pathways (Westoby et al., 2012, 2014b; Wilson et al., 2019). Numerical hydrodynamic simulation has been successfully applied to model downstream GLOF passage (Worni et al., 2014; Westoby et al., 2014b; Sattar et al., 2019; Wilson et al., 2019) and provide estimates of transient flow characteristics including inundation flow depth and extent, and flow velocity, which are useful for developing hazard maps and estimating historical or future damage and losses under various outburst scenarios.

This study aims to: (1) reveal the evolution of glacial lakes within the Chongbayong catchment using satellite imagery captured between 1987 and 2019; (2) simulate the Chongbaxia Tsho moraine dam breach and GLOF using a 1-D (dimensional) dam breach model and a MATLAB-based 2D hydrodynamic numerical simulation, and which incorporates field survey data, including DEM data captured from a UAV, and satellite observations; (3) analyze the downstream impact of this GLOF event, and; (4) discuss the future status of Chongbaxia Tsho considering glacier change and topographic characteristics. On a wider level, this study seeks to provide valuable insights into GLOF hazard modeling and risk assessment in the Himalayas.

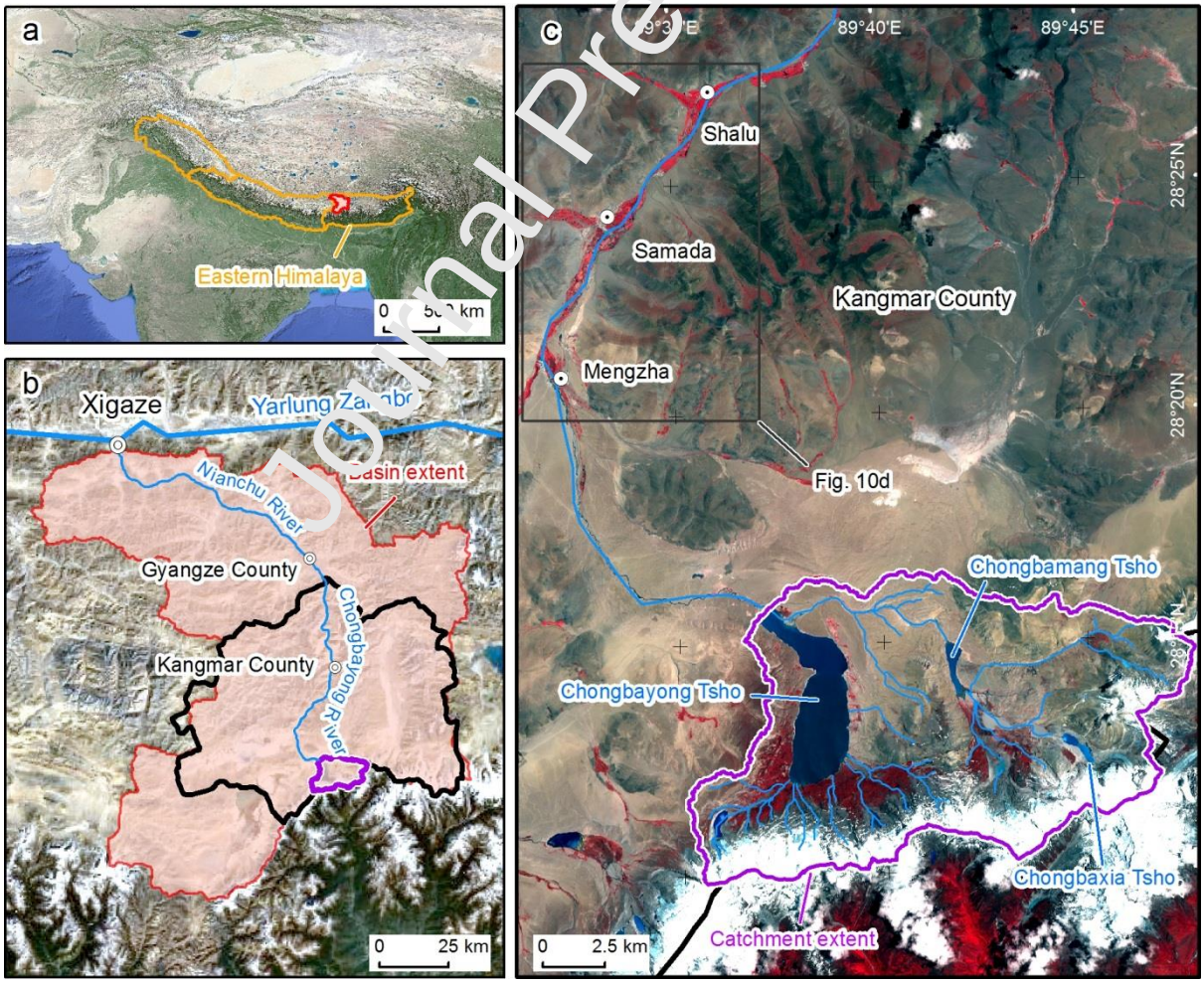

Fig. 1. Location of the study area: (a) location of Nianchu River basin in the Eastern

Himalaya, (b) location of Kangmar County (black line), Chongbayong River, and the study catchment (purple line), (c) Kangmar County and the location of the study site within this region. The extent of Fig. 10d is also marked. Background in (a) and (b) are ©ESRI, and background imagery in (c) is Sentinel-2 imagery acquired on 24 June, 2019.

2. Study area

The study area is the Nianchu River basin, Kangmar County, which is located in the eastern Himalaya between Bhutan and Tibet, China. Specifically, we focus on the upper catchment where Chongbaxia Tsho, Chongbamang Tsho and Chongbayong Tsho are situated (**Fig. 1**). Chongbayong River originates from the main range of the eastern Himalaya as an upper tributary of Nianchu River, which in turn is a tributary of the Yarlung Zangbo (**Fig. 1**b). Settlements and human activities are mainly distributed along the rivers (**Fig. 1**c). The total population of Kangmar County was approximately 22,900 in 2016. The climate in the study area is driven dominantly by Indian summer monsoon and westerlies (Bohner, 2006) and the precipitation regime shows a south-north gradient due to the orographic barrier effect of the Himalayas (Bookhagen and Burbank, 2006; Nie et al., 2017). The mean annual air temperature and precipitation between 1987 and 2018 are, respectively, 5.5℃ and 279.7 mm at the nearest Gyangze County station.

Chongbaxia Tsho (28.211°N, 89.745°E) is a moraine-dammed lake with an area of 0.46 km^2 in 2019. Its catchment area is ~12.6 km^2, including a glacierised area of 6.1 km^2 and an estimated ice volume of 1.6×10^8 m^3 based on ice thickness mapping (Farinotti et al., (2019); Randolph Glacier Inventory (RGI Consortium, 2017) ID: RGI50-13.26449 with a glacier area of 3.9 km^2). A GLOF originating in the Chongbayong catchment was first documented as occurring during 2000-2001, but the source lake was unknown. Another two studies predicted

that it likely occurred on 6 August 2000 and originated from Longjiu Tsho or Chongbaxia Tsho. A recent study confirmed that the most likely source was Chongbaxia Tsho, and that the GLOF occurred in 2001 and was associated with moraine dam failure; an erosion gully in the moraine with a maximum width of 90 m is visible on satellite imagery. However, knowledge of the growth of Chongbaxia Tsho and evolution of the 2001 GLOF are poorly understood. Flow from the Chongbaxia Tsho catchment enters Chongbamang Tsho (with a catchment area of 73.7 km^2) approximately 4.5 km downstream, before reaching Chongbayong Tsho a further 8.5 km downstream (an ancient glacial lake with a catchment area of 169.4 km^2 and also named Chumba Yumco). The elevation range of the Chongbayong Tsho catchment is 4530 - 6210 m a.s.l according to a PALSAR DEM derived from L-band Synthetic Aperture Radar (ASF DAAC, 2015). There are 15 glaciers with a total area of 24.4 km^2 in 2010 in the Chongbayong Tsho catchment, and the glacierised area covers an altitudinal range of 4856 to 6044 m according to the second Chinese Glacier Inventory (CGI) (Guo et al., 2015). An artificial dam complex, including a primary dam (576 m-long) and an auxiliary dam (298 m-long), exists at the outlet of the Chongbayong Tsho reservoir and regulates downstream flows for irrigation, flood prevention and eco-environmental conservation. Dam construction began in 1986, and it became operational in 1989. It was repaired in 2006. The total water volume of Chongbayong Tsho is approximately 660×10^6 m^3. Chongbaxia Tsho therefore represents the upper component of a river-lake cascade, which makes it particularly unique in terms of the implications for downstream GLOF passage and potential attenuation.

3. Material and methods

3.1. Datasets

Remotely sensed data from multiple satellite platforms were used in this study. A total of 36 Landsat images (U. S. Geological Survey, 2016) with a consistent spatial resolution of 30 m between 1987 (earliest available imagery) and 2016 were used to extract lake and glacier extents. Six Sentinel-2 scenes with a spatial resolution of 10 m for multispectral bands were retrieved between 2016 and 2019 (Copernicus, 2019) and were also used for lake and glacier mapping (Table 1S). All imagery are provided as terrain-corrected products and well matched with an error of around 0.5 pixels pixel (15 m for Landsat data and 5 m for Sentinel data). Planet images with a spatial resolution of 3 m (15 scenes, 2016-2019) were used to aid georeferencing of UAV data, and for monitoring glacial dynamics (Planet Team, 2017).

Field surveys were performed on 21 and 22 October 2016 with the aim of investigating the geomorphological characteristics of the Chongbaxia Tsho moraine dam and wider lake basin, and impacts related to the GLOF, specifically the moraine breach, a perched shoreline (as an indicator of the pre-GLOF lake level), river- and rock-bed topography, and the downstream depositional and erosion signature of the outburst. A UAV survey was carried out on 22 October, 2016 with the aim of acquiring photos for the construction of a high-resolution orthomosaic and digital surface model (DSM) covering the moraine dam and immediate downstream area (**Fig. 2**a and b). A total of 417 photographs at the end moraine zone were taken using a 12-Megapixel camera (DJI FC330) installed on DJI Phantom 4 UAV. Photograph capture mode was set to ‘shutter priority’ (1/1000s) in order to reduce image blur.

DEM data and DEM differencing methods are essential tools for quantifying landscape change across large spatial scales, and for this reason are important components in glacial hazard assessment (Westoby et al., 2014b; Lala et al., 2018); DEM topography is required for hydrodynamic GLOF simulation, and DEMs of difference (DoD) can be used to quantify erosion and deposition along a GLOF flow path, and analyze landscape change in glacial lake catchments. DEM data that are useful for these purposes include those generated by the Shuttle Radar Topography Mission (SRTM, open access), and the proprietary TanDEM-X DEMs, the latter of which have global coverage at 12 m resolution, has an absolute vertical error of <2 m at 90% confidence (Wessel et al., 2018) and shows promising potential for mountain geomorphological research more broadly (Boulton and Stokes, 2018). Newer, freely available, DEMs such as the PALSAR-DEM (12.5 m resolution (Niipele and Chen, 2019)) and the 8 m-resolution High Mountain Asia (HMA) DEM (Shean, 2017) offer more flexible, high-resolution alternative to lower resolution, or expensive, data products. In this study we evaluated the suitability of an SRTM DEM (V3, acquired 11-22 February 2000 (Farr et al., 2007)), a PALSAR DEM acquired 21 June, 2008, (ASF DAAC, 2015), a HMA DEM dated 6 October, 2015 (Shean, 2017), and TanDEM-X data acquired between 2011 and 2015 (Grohmann, 2018) to estimate pre- and post-GLOF lake water volume, and provide topography for downstream GLOF routing (Table 1).

We also used: annual and monthly meteorological data at Gyangze County between 1987 and 2018 from the China Meteorological Administration to analyze the role of climate change in GLOF hazard evolution; CGI data (Guo et al., 2015) for baseline data on glacier extent;

existing elevation change data (Brun et al., 2017) for validating our estimates of the water volume released by the GLOF, and; glacier thickness data (Farinotti et al., 2019) for considering the role that future glacier evolution might play in terms of conditioning an environment which might produce GLOF triggers.

Table 1 Characteristics of DEMs used in this study

Data	Acquisition date	Spatial resolution (m)	Imaging system
SRTM DEM	February, 2000	30	SAR C band
PALSAR DEM	21 June, 2008	12.5	SAR L band
TanDEM-X	2011-2015	90	SAR X band
HMA DEM	6 October, 2015	8	Optical

3.2. Methods

3.2.1. Validation of GLOF event, glacier and glacial lake mapping

Diagnostic landscape characteristics that are critical for validating the occurrence of a GLOF include the obvious shrinkage of lake extent (implying drawdown), the identification of a moraine breach or trench (generally carved over a short duration by escaping floodwater), evidence of downstream erosion in the form of significant in-channel and overbank scour (indicative of the passage of a high-magnitude flow), and depositional features, such as a debris fan that originates from a breach (Nie et al., 2018; Veh et al., 2019). By identifying all of these geomorphological features and the date at which they appear in historical satellite imagery, and later validating these through field investigation, Nie et al (2018) confirmed an outburst from Chongbaxia Tsho as occurring sometime between 5 February and 4 November, 2001. Glacial lake and glacier extents in the study area were extracted using an advanced

automated adaptive lake mapping method based on Landsat and Sentinel images (Wang et al., 2014; Sheng et al., 2016; Nie et al., 2017; Wang et al., 2017; Jiang et al., 2018; Yao et al., 2019). Specifically, the Normalized Difference Water Index (NDWI) (Mcfeeters, 1996) was used to derive glacial lake extent while the Normalized Difference Snow/Ice Index (NDSII (Hall et al., 1998) was used to extract glacier extent. Specifically, we first calculated the NDWI and NDSII histograms in each region of interest, and then interactively set the threshold to extract lake or glacier extent based on instantaneously screening boundary in the images. A further consideration is that inland water (lake and river) masks are widely applied during DEM generation to void-fill in these regions because of the very low reflectivity of undisturbed water (USGS, 2015). There is therefore uncertainty regarding the accuracy of the water surface elevation as it is represented in these DEM products, because inland lake extents can fluctuate both temporally and spatially. However, we consider that this effect is minor for most glacial lakes, which tend to have an outflow channel that regulates a more-or-less constant lake level. To take these factors into account, we calculated the final lake volume decrease by using a combination of lake extents, lake level change and topography. We anticipate that these factors will become less of a consideration as more accurate, and higher resolution DEMs become available for remote regions.

Lake and glacier outlines were exported as shapefiles. An error of ±0.5 pixels (15 m for Landsat data and 5 m for Sentinel data) is associated with the perimeter of each extracted glacial lake and glacier (Nie et al., 2017; Jiang et al., 2018) and was used to calculate the mapping uncertainty.

3.2.2. UAV processing

Structure-from-motion (SfM) photogrammetry methods (Westoby et al., 2012, 2014b; Vargo et al., 2017) were implemented in Pix4Dmapper (v2.1) software (Colomina and Molina, 2014; Terwisscha Van Scheltinga et al., 2020) and were used to generate a DSM and orthomosaic from our UAV data. For computational efficiency we set image scaling at 0.5 and 'optimal mode' was selected for point density during point cloud and mesh reconstruction – the latter is useful for guiding GCP placement. We used photograph geo-tags to assist with initial camera pose estimation and sparse point cloud reconstruction, and provide key information (e.g. focal length) for camera calibration. The mean number of matched 2D key-points was ~21,000 per image and the relative difference between parameters in an initial and an optimized camera model was <5%. Due to field constraints, we could not deploy and survey a well-distributed ground control network and so as an alternative we manually identified 15 stable features to use as GCPs from a Planet image acquired on 23 October, 2016, one day after the UAV survey, and which is the highest resolution, freely available optical satellite imagery for the site. We extracted x and y GCP co-ordinates from this satellite imagery, and retrieved z information from a PALSAR DEM, which was chosen due to its high (12.5 m) resolution. GCPs were imported in the WGS84 UTM (zone 45N) coordinate system (**Fig. 2**a). The mean positional accuracy of these GCPs following placement and bundle adjustment was 0.01 m, -0.03 m and 0.07 m in xyz, implying a high degree of internal model consistency. We assume that the relative geo-location error is ±2 m at 98% confidence, which is in line with a handheld GPS-estimated value of vertical

difference for control point locations. We note that our method of using a satellite-derived DEM and imagery for extracting GCP information where no accurate, field survey-derived control data are available has also been used in other similar studies, such as Wilson et al., (2019).

We generated a DSM at 0.13 m grid spacing from our dense point cloud (totaling 25×10^6 densified 3D points), and used 'sharp' surface smoothing and the 'Inverse Distance Weighting' method rather than 'Triangulation' for DSM generation in Pix4Dmapper because the former is more suitable for reconstructing rugged terrain. We determined the elevation of the pre-GLOF lake surface by combining field- and remote sensing-based observations; specifically, we used the UAV orthoimage and DSM to extrapolate post-GLOF field observations of the location of the perched shoreline, and validated this mapping using knowledge of maximum lake extent from pre-GLOF Landsat satellite imagery from 2001. We further used the UAV orthoimage to map the current lake extent, which was later used in combination with a satellite-derived DEM to determine lake level decrease and estimate the initial GLOF volume (see section 3.2.3). We discuss uncertainties relating to our estimate of pre- and post-GLOF lake levels as they relate to reconstructing the volume of the GLOF in section 3.2.3.

3.2.3. DEM uncertainty and estimation of flood volume

We used SRTM DEM data to represent the pre-GLOF topography of the study site because these data were acquired approximately one year before the outburst and are

therefore the best topographic representation that is available for this point in time. To validate the elevational accuracy of the SRTM DEM, we compared it with other, more recent DEMs that have a higher product accuracy. A total of 100 random points were generated on stable ground (excluding water bodies, snow and glacier cover) around Chongbayong Tsho catchment (**Fig. 2**c, and d), and for which DEM elevation was extracted. Linear regression showed that all DEMs had a significant relationship (Adj. R^2 >0.999). The mean difference between the PALSAR DEM and TanDEM-X was 2.36 m compared to 1.52 m between the PALSAR and HMA DEMs. The median is <2 m for both comparisons. We observed a median difference of 30 m between the PALSAR and SRTM DEMs, a shift which is probably caused by a systematic elevation bias of the latter DEM in the study area (**Fig. 3**). We therefore subtracted 30 m from the SRTM DEM, and used this topography as an input for GLOF simulation in this study. The mean difference between the z-shifted SRTM and PALSAR DEMs was 0.51±4.25 m (1 σ) (**Fig. 3**). Whilst we acquired a handheld GPS trace at the site, these data are not spatially (or topographically) representative of the wider site and were therefore only used for field mapping. Further, because these data were collected in a format that could not be differentially corrected, which would improve their accuracy, it is highly unlikely that the xyz accuracy of these data exceeds the relative accuracies of our DEM products (see inset tables in Fig. 3), which we instead feed forward into our uncertainty estimation of the drained lake volume.

Considering the coarse resolution (90 m) of TanDEM-X data and the extensive areas of no data in the corresponding HMA DEM across the study site, we used the PALSAR DEM to

represent the post-GLOF topography for the catchment. By vertically differencing the z-shifted SRTM and PALSAR DEMs we estimated the volumetric difference between the lake marginal topography which was previously submerged, and which emerged as the lake level dropped to be 2.5×10^6 m^3. If we extract volume loss for the same spatial extent from Brun et al.'s (2017) elevation change map for HMA, which was derived from the differencing of SRTM and co-registered ASTER DEM data (a differencing period of 2000-2016), we produce a volumetric change of 2.7×10^6 m^3, which is a difference of 6.9%, demonstrating a high degree of consistency between our estimate of lake volume decrease and that estimated using secondary data. By subtracting the PALSAR DEM-derived elevation of the current lake surface from our SRTM DEM-derived estimate of the pre-GLOF lake surface elevation, we estimated that the lake level decreased by 37±2 m as a result of water volume loss associated with the GLOF, and where our uncertainty bound encompasses the residual vertical error between the pre-GLOF (SRTM) and post-GLOF (PALSAR) DEM topography (**Fig. 2**a, and b).

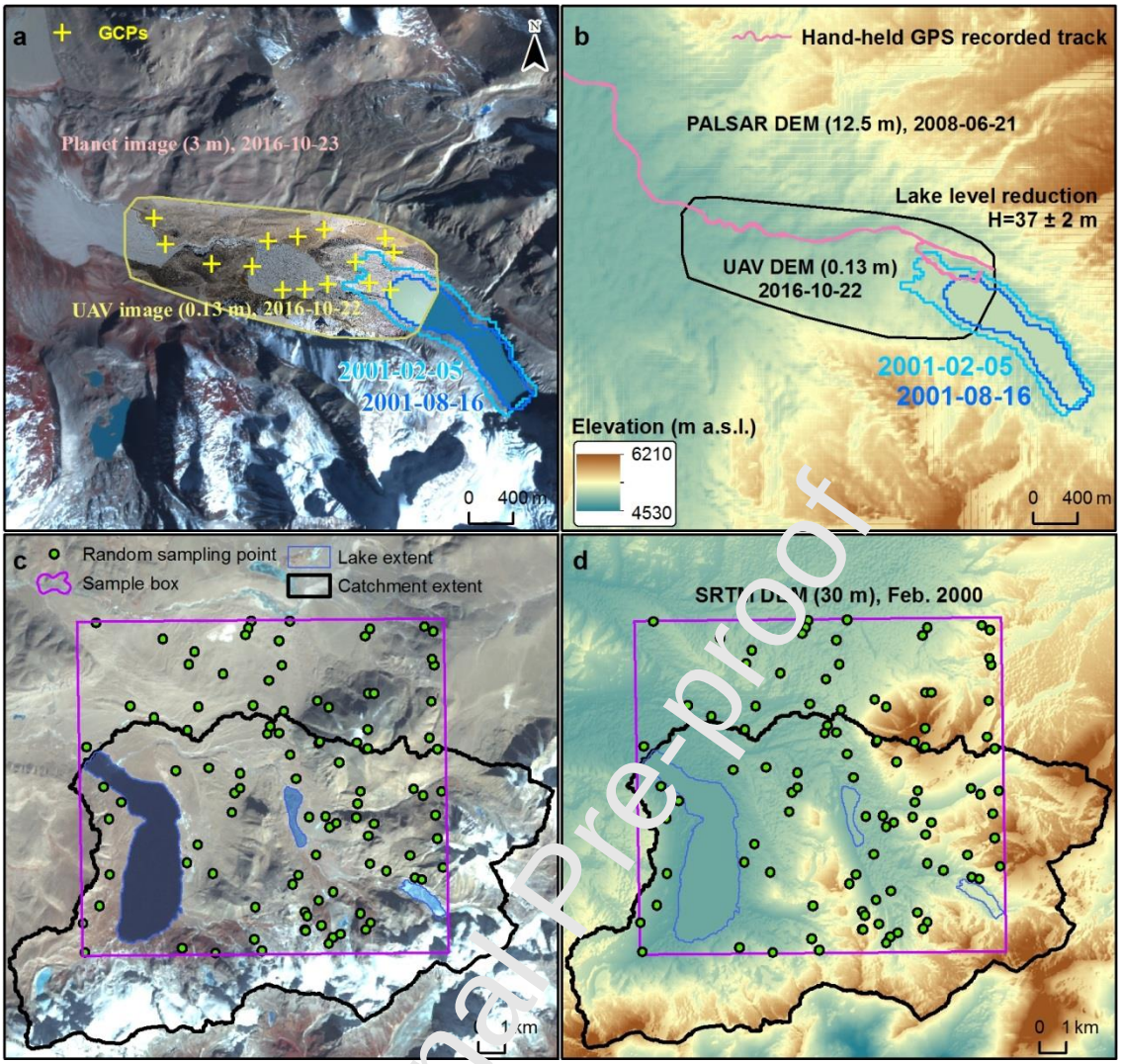

Fig. 2. High resolution imagery and DEM data products for the study area. (a) ortho-rectified high resolution images of Planet image on 23 October, 2016 (background) and our UAV-derived orthoimage of the moraine and immediate downstream area, derived from imagery captured on 22 October 2016 and processed using SfM methods, (b) PALSAR DEM and UAV-derived DEM extent overlaid with a field-recorded GPS route, (c, d) spatial distribution of random sampling points on stable surfaces which were used to quantify elevational differences between various DEMs. Background image in (c) is a Landsat image acquired on 19 December 2000. Background topography in (d) is a SRTM DEM.

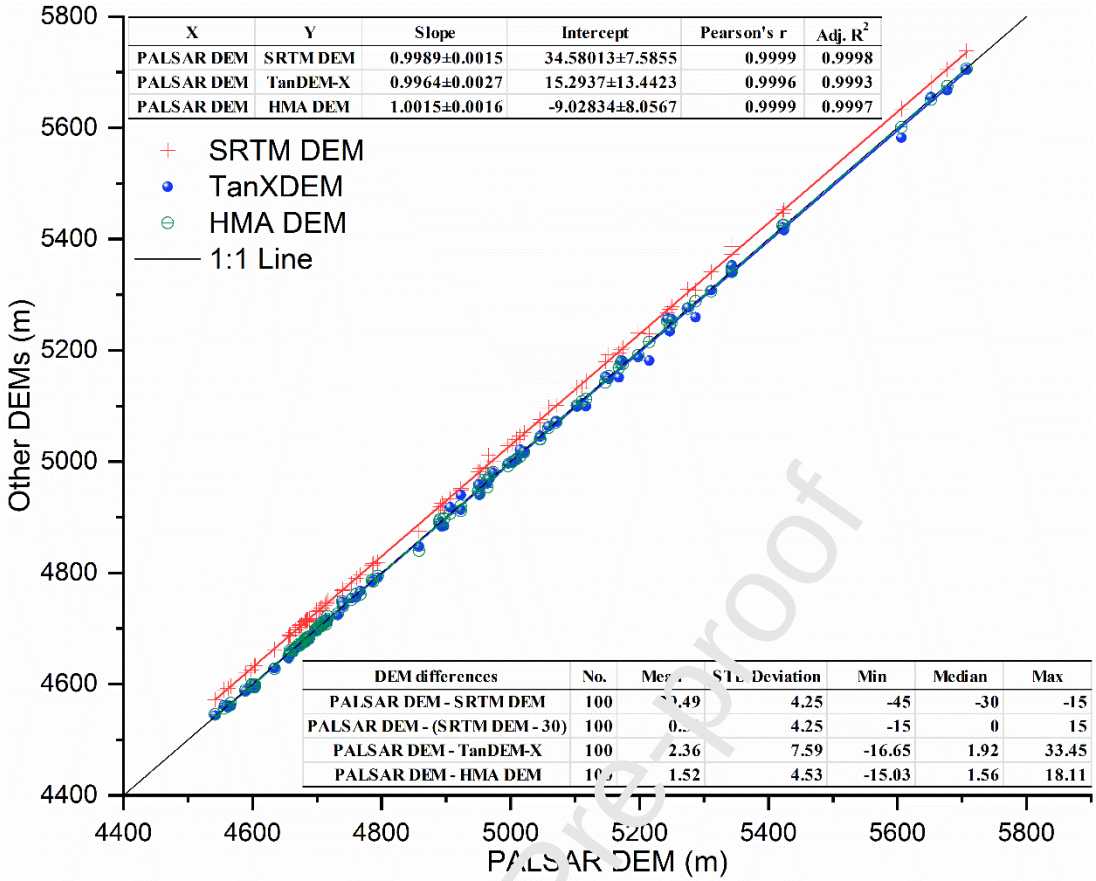

Fig. 3. Comparison of DEM elevations for random points (**Fig. 2**c, d).

3.2.4. GLOF simulation

A range of software packages have been used to simulate dam-breach formation and downstream GLOF propagation, and each has their own advantages and shortcomings. Models that have been used to date include NWS BREACH (Wang et al., 2008; Worni et al., 2014), HR BREACH (Westoby et al., 2014b, 2015), Dam/Levee Breach (DL Breach) (Wu and Wang, 2007; Wu, 2016), HEC-RAS (Wang et al., 2018; Sattar et al., 2019), BASEMENT (Lala et al., 2018; Vetsch et al., 2020), FLO-2D (Worni et al., 2014), and r.avaflow (Mergili et al., 2017) and most those have a hydrodynamic component which is based on the shallow water equations (SWE). Designing a GLOF simulation is generally a compromise between

input data availability, computational cost (which is often determined by the dimensionality and physicality of the model), model robustness, and the desired quality and detail of the data outputs (Westoby et al., 2014a).

Our GLOF simulation workflow is comprised of two stages: 1) dam breach simulation, and 2) downstream GLOF propagation. To generate a dam-break hydrograph we used the physically-based numerical model DL Breach, which employs a 1D non-equilibrium total load equation to simulate the evolution of breach morphology and solves the governing shallow water equations for simulating flow over the dam using an explicit finite volume method (Wu and Wang, 2007; Wu, 2016). DL Breach shares similarities with a number of the models referenced above (like HR BREACH, it simulates breach erosion in the form of head-cut migration) but with additional capability to simulate the development of scour holes in the breach as it develops, and the ability to simulate sub-base erosion (Zhong et al., 2016). Key model input parameters include embankment geometric characteristics, breach 'mode', Manning's *n* value for surface roughness, an initial upstream and downstream water surface level, final breach bottom width, outflow water volume and lake area. We tested three scenarios of lake level decreases: 35 m, 37 m and 39 m, which represented upper and lower initial GLOF volumes of 28.7×10^6 m^3 and 25.5×10^6 m^3, respectively. In the absence of any definitive evidence to suggest otherwise, we assume that the mode of breach initiation was via overtopping, which is in line with the vast majority of documented moraine-dam failures worldwide, and that the moraine has a non-cohesive dam structure, which we confirm via field investigation (**Fig. 4**). A simulation is initiated by specifying a lake level which is above

the crest of the dam, followed by the implementation of a weir formula for routing flow over the dam crest and initiating incision.

To select an optimal set of initial conditions, we ran a series of dam breach scenarios and compared the modelled maximum breach top width with field data, and, in the absence of any field measurements of breach outflow during the GLOF, an estimate of peak discharge derived from an independent equation that uses lake volume as a key input (Evans, 1986). Assuming a water level decrease of 37 m, and a total outflow volume of 27.1×10^6 m^3 we produced a modelled peak discharge of 6625 m^3 s^{-1}. The peak discharge as estimated using Evans' equation (1986) is 6267 m^3 s^{-1}. We therefore find a volumetric difference of 5% between our numerical modelling derived estimate, and an estimate from a well-established empirical equation; such empirical equations have been routinely used to estimate GLOF discharge characteristics for sites where a lack of field data precludes the use of more advanced methods (Westoby et al., 2014a), but the use of such equations is becoming less common. The maximum modelled breach top width was 92 m, which is a difference <2% when compared to the same metric extracted from the UAV orthoimage. The breach outflow hydrograph for a total water level drop of 37 m (Fig. 4) was exported for use as input for our flood propagation model.

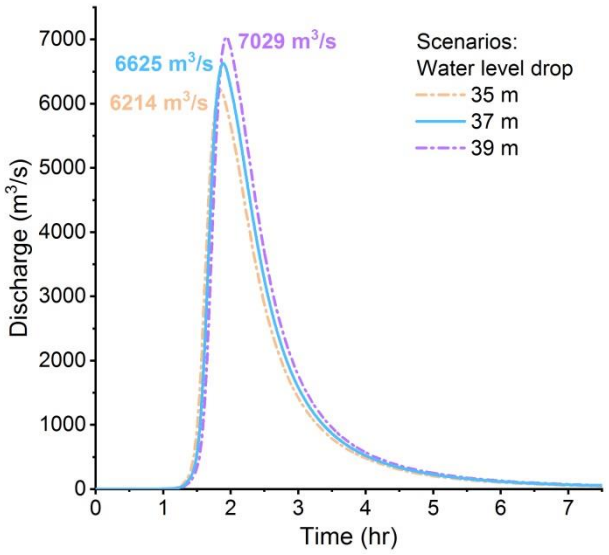

Fig. 4. Modelling-derived hydrograph at the moraine breach. The hydrograph was constructed using the 1D DL Breach model for three initial lake level scenarios based on water level decrease uncertainty.

We simulate GLOF propagation between the moraine breach and Chongbayong Tsho, a distance of approximately 15 km, using a MATLAB-based 2D model, and which adopts the classic SWE. The model and its main principles have been described in detail by Liang (2010) and have been successfully applied to simulate flood propagation (Liang, 2010; de Almeida et al., 2012; Worni et al., 2013; Vacondio et al., 2014). The model conserves both mass and momentum, which are expressed as:

$$\frac{\partial h}{\partial t}+\frac{\partial}{\partial x}(hu)+\frac{\partial}{\partial y}(hv)=0 \tag{1}$$

$$\frac{\partial}{\partial t}(hu)+\frac{\partial}{\partial x}\left(hu^2+\frac{1}{2}gh^2\right)+\frac{\partial}{\partial y}(huv)=-gh\left(\frac{\partial z}{\partial x}+S_{fx}\right) \tag{2}$$

$$\frac{\partial}{\partial t}(hv)+\frac{\partial}{\partial x}(huv)+\frac{\partial}{\partial y}\left(hv^2+\frac{1}{2}gh^2\right)=-gh\left(\frac{\partial z}{\partial y}+S_{fy}\right) \tag{3}$$

where h is flow depth; u and v are the flow velocity components; g is the gravity acceleration; z is the bed elevation; S_{fx} and S_{fy} are the Manning friction terms, and can be expressed as:

$$S_{fx} = gn^2 u\left(u^2 + v^2\right)^{1/2} h^{1/3}$$
$$S_{fy} = gn^2 v\left(u^2 + v^2\right)^{1/2} h^{1/3} \quad (4)$$

where n is the Manning friction coefficient.

A notable caveat is that the model does not consider the effect of sediment erosion and deposition, or the 'mobile bed' phenomena, and is thus limited to simulation of clear water flows. The model employs a finite volume method coupled with an approximate (Harten-Lax-van Leer-Contact) Riemann solver, which can handle the discontinuous problem at the grid cell interface well (Liang and Borthwick, 2009). A well-balanced scheme proposed by Audusse et al (2004) was used for preserving a steady state at the discrete level and preventing a non-physical flux. Our z-shifted SRTM DEM was used to represent the downstream topography, over which the flood was routed. The friction coefficient n, is a key parameter of the Manning equation (Wilson et al., 2019), affecting the flow propagation. In our modelling workflow, the lake water in Chongbamang Tsho and Chongbayong Tsho is considered immobile, and the lake surface is considered as a topographic surface over which the GLOF is routed, and which is a limitation of our method. The n values for lake water and non-water surfaces are greatly different. Therefore, two values of n, 0.05 for non-water surface and 0.02 for lake water surface were used according to previous studies (Westoby et al., 2014b; Sattar et al., 2019).

4. Results

4.1. Chongbaxia Tsho GLOF event and relevant lake changes

The specific date of the Chongbaxia Tsho GLOF event probably occurred on 6 August

2001. The maximum extent of the lake in the satellite imagery record was 0.80 km^2, which was observed on 5 February 2001, and was the culmination of rapid expansion since 1987 (Fig. 5). By 16 August 2001 the lake area had decreased to 0.34 km^2 as a result of dam failure (**Fig. 5** and **Fig. 6**). We narrowed the timing of the GLOF to between 31 July and 8 August 2001 through the evidence of changes in lake extent, downstream vegetation and sedimentary deposits before and after flooding interpreted from the images. We refine the actual date of the Chongbaxia Tsho event to be 6 August 2001, not 6 August 2000, as previously believed (Liu et al., 2016).

Analysis of lake area changes of Chongbaxia Tsho, Chongbamang Tsho and Chongbayong Tsho between 1987 and 2019 sheds light on the impacts of the GLOF, and in the case of Chongbayong Tsho, management decisions that were made as a direct result of the 2001 event. Pre- and post-GLOF trends in lake area were revealed through satellite observations acquired between 1987 and 2019 (**Fig. 5**). Before the dam failure of Chongbaxia Tsho, the lake area of Chongbayong Tsho and Chongbaxia Tsho had been continuously increasing since 1987, meanwhile Chongbamang Tsho was stable with a mean area of 0.83±0.07 km^2. Immediately after the 2001 GLOF, the area of Chongbaxia Tsho and Chongbayong Tsho rapidly shrank and reached their lowest historical water level on 16 August and 4 November 2001, respectively. The area of Chongbaxia Tsho was stable between 2002 and 2019 with a mean area of 0.47±0.04 km^2 (**Fig. 5**) while Chongbayong Tsho expanded by 12.8% between 2002 and 2006. Following the GLOF, it appears that the level of Chongbayong Tsho was either artificially reduced to its minimum extent of ~11 km^2 in

November 2001 to mitigate against overflow whilst repairs to the structure were carried out, or damage to the dam caused the uncontrolled release of additional lake water, although we cannot confirm the exact cause for this sudden drop. Since 2006 the level of the reservoir has fluctuated as a result of regulation to meet the downstream water demands (Fig. 5). The area of Chongbamang Tsho did not contract immediately after the GLOF, but its level steadily declined after 2002 to a minimum area of 0.65 km^2 in 2007. Its area was remained relatively stable between 2002 and 2019 with a mean area of 0.71±0.06 km^2.

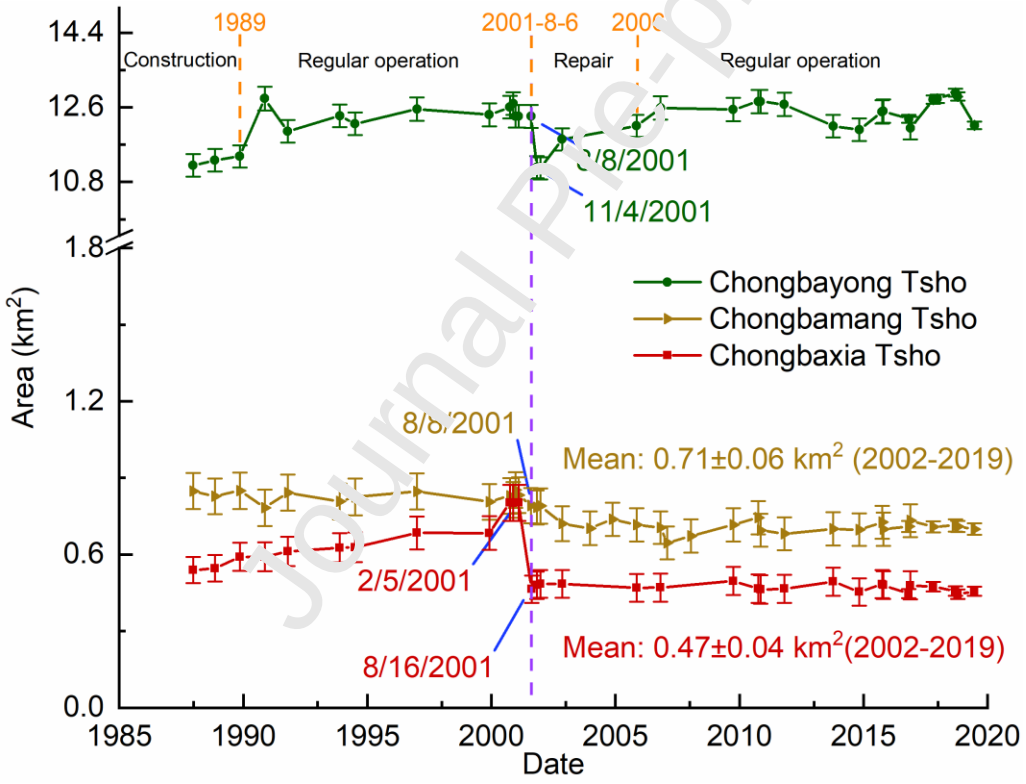

Fig. 5. Surface area changes for the three lakes in the study catchment from 1987 to 2019.

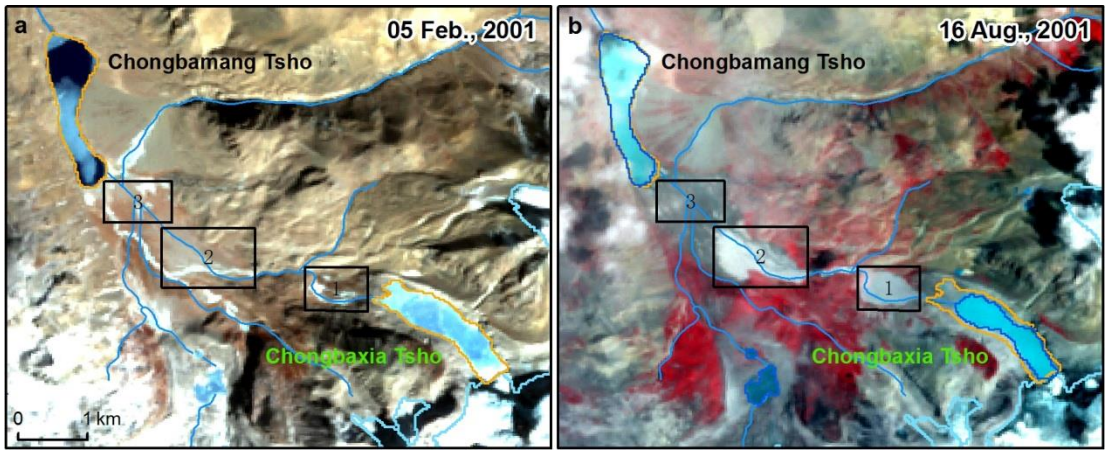

Fig. 6. Changes in the surface area of Chongbaxia Tsho moraine-dammed lake, and along the GLOF flow path, between Feb. and Aug. 2001, including the effects of the 2001 GLOF. The pre-GLOF lake extent on 5 February 2001 (yellow line) was selected as the reference for comparing the changes. Background data are Landsat images displayed in standard false color composite (near-infrared, red, and green as RGB). Black rectangles highlight sudden landscape modification (i.e. development of debris fans) as a result of the 2001 GLOF.

4.2. The 2001 Chongbaxia Tsho GLOF

A total water volume of 27.1±1.6 × 10^6 m^3 was released from Chongbaxia Tsho in 2001. Summary outputs for our modelled reconstruction of the GLOF are shown in Figs. 7-9. Assuming a maximum lake level drop of 37 m, the GLOF flow depth, velocity and peak discharge greatly varied both temporally and spatially (**Fig. 7-9**) in the first 10 hours after the initiation of dam failure according to our simulation. The maximum modelled flow depth was 20.4 m and occurred near the breach site at 1.87 h since breach development (Fig. 7), and the maximum modelled flow velocity was 17.8 m a^{-1}, which occurred at 1.4 km from the breach

at 1.95 h. Generally speaking, the momentum of the GLOF gradually reduces with distance from the breach, primarily due to the effects of land surface friction. Localised increases and decreases in flow depth and velocity along the flood path are the product of flow constrictions and expansion as a result of the topography; inundation depths and flow velocities increase in narrow channels and decrease as the floodplain widens (**Fig. 7** and **Fig. 8**). However, the Chongbayong Tsho dam and flow dispersion across the fixed surface topography of Chongbamang Tsho and Chongbayong Tsho greatly attenuated the GLOF in this study; the flow velocity obviously decreased between at 2.2 h and 3.1 h, and the peak discharge noticeably decreased from cross-section B at 4.1 km downstream of the breach to cross-section C at 12.8 km downstream (**Fig. 8** and **Fig. 9**).

Our simulations suggest that the GLOF reached Chongbamang Tsho approximately 1.9 hours after the beginning of breach 'initiation', i.e. the phase during outflow discharge is typically very low, and during which time runaway breach development is still uncertain and preventable. The modelled GLOF reached Chongbayong Tsho at ~3.1 h (**Fig. 7** and **Fig. 8**). We estimate that Chongbayong Tsho stored roughly 96% of the total flow volume (**Fig. 9b**) and released the excess floodwater through a small water outlet (less than 10 m wide). The widened river (maximum 500 m in width) and inundation zones downstream from the Chongbayong Tsho dam were observed in the Landsat images acquired on 8 and 16 Aug. 2001. It appears that it took several days for the lake level in Chongbayong Tsho to stabilize, which we infer from the lake extent fluctuations immediately after the event (**Fig. 5**).

Chongbamang Tsho and Chongbayong Tsho played a crucial role in buffering against

the cascading nature of the Chongbaxia Tsho GLOF, as shown through the changes in flow depth, velocity and peak discharge along the flood path. The significance of the second of the two lakes in the cascade, Chongbamang Tsho, is evidenced in Fig. 9, which shows that additional water storage increases in this lake rapidly as the GLOF reaches it, but that the volume is then released gradually over a period of many hours. The additional water volume stored in the Chongbayong Tsho reservoir increases as soon as the GLOF reaches this water body. The total water storage of Chongbamang Tsho converted from increase to decrease, and reached its maximum at 3.4 hours after the dam-break in accordance with the hydrograph at cross-section B (Fig. 9). The total stored water volume of Chongbayong Tsho increased gradually as the result of continuous water inflow and the obstruction of its concrete dam. Passage of the GLOF through Chongbamang Tsho slowed its flow velocity and indirectly reduced damage to the Chongbayong Tsho dam, which in turn buffered the GLOF and greatly reduced its downstream destructiveness.

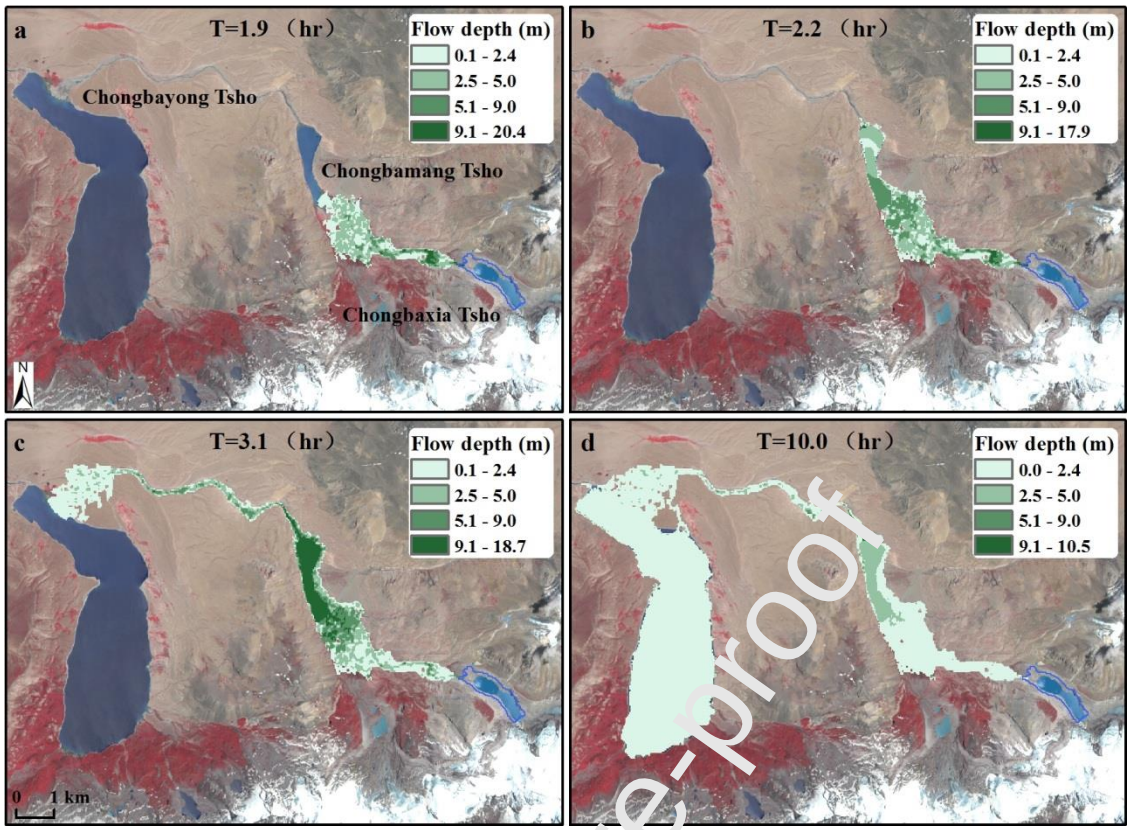

Fig. 7. Modelled flow depth of the 2001 Chongbaxia Tsho GLOF event for various time steps, specifically the points at which the GLOF reaches (a) the upstream limit of Chongbamang Tsho, (b) the outflow of Chongbamang Tsho, (c) Chongbayong Tsho, (d) simulation end. Background is a Sentinel-2 image acquired on 24 June 2019. Also shown is the pre-GLOF extent of Chongbaxia Tsho (blue line) on February 5, 2001.

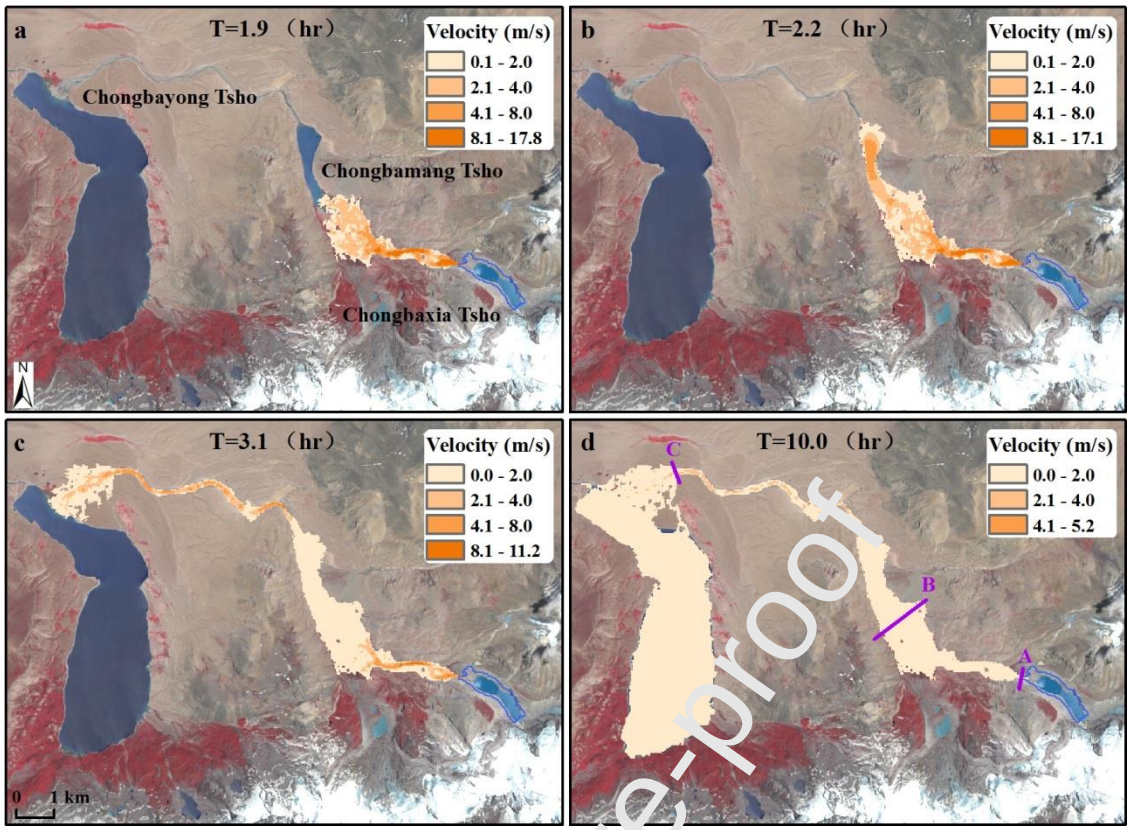

Fig. 8. Simulated flow velocity of Chongbaxia Tsho GLOF event on Aug. 6, 2001 at different time steps (see Figure 7 caption for explanation). Also shown in (d) is the location of three cross-sections (A-C) for which hydrographs are shown in Fig. 9. Background image is as per Fig. 7.

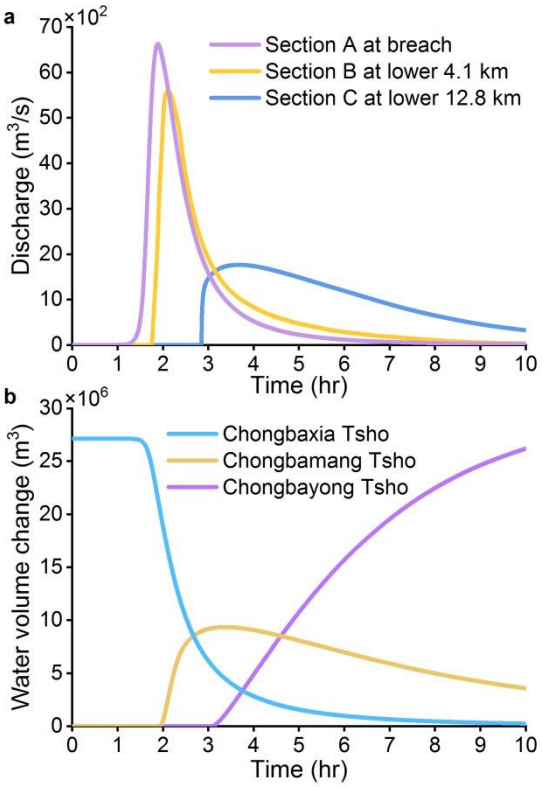

Fig. 9. Modelled GLOF discharge at three critical cross sections along the flow path (Fig. 8d), namely the moraine breach (section A), immediately upstream of the second lake in the cascade, Chongbamang Tsho (section B), and the upstream boundary of Chongbayong Tsho (section C); (b) water volume change of Chongbaxia Tsho, Chongbamang Tsho and Chongbayong Tsho during the first 10 hours of the GLOF.

4.3. Downstream impacts of the GLOF

The GLOF destroyed 346.4 ha of valuable meadowland between its source and the Chongbayong Tsho dam (**Fig. 10**a and b) which we infer from a manual visual comparison of pre- and post-GLOF vegetation coverage adjacent to the river (23 July 2001) which was freshly scoured by the GLOF, leaving fresh boulder and sand deposits as shown on Landsat imagery, and validated during field investigation (**Fig. 6** and **Fig. 10**). The GLOF partly

damaged the Chongbayong Tsho dam (**Fig. 10**c) because the excess floodwater exceeded its design overflow capacity. The GLOF posed a hazard to local residents up to 60 km downstream from its source, although no fatalities were reported. Some buildings were abandoned immediately downstream of Chongbaxia Tsho following the event (Fig. 10a). The Chongbayong Tsho dam played a crucial part in buffering the potential impact of the GLOF further downstream, including loss of life and injury, and wider economic impact. As a result of damage caused by the GLOF, the dam had to be repaired and upgraded at an estimated cost of >2 million USD. Approximately 151.3 ha of croplands were destroyed along the Chongbayong River between the Chongbayong Tsho dam site to the boundary between Kangmar and Gyangze counties, a distance of 45 km. The most severe inundation zones were mainly distributed at the river sections between Mengzha and Salu (**Fig. 10**d). Specific socio-economic losses for the event remain absent due to difficulties associated with a lack of accurate reporting and communication in such a remote area around two decades ago.

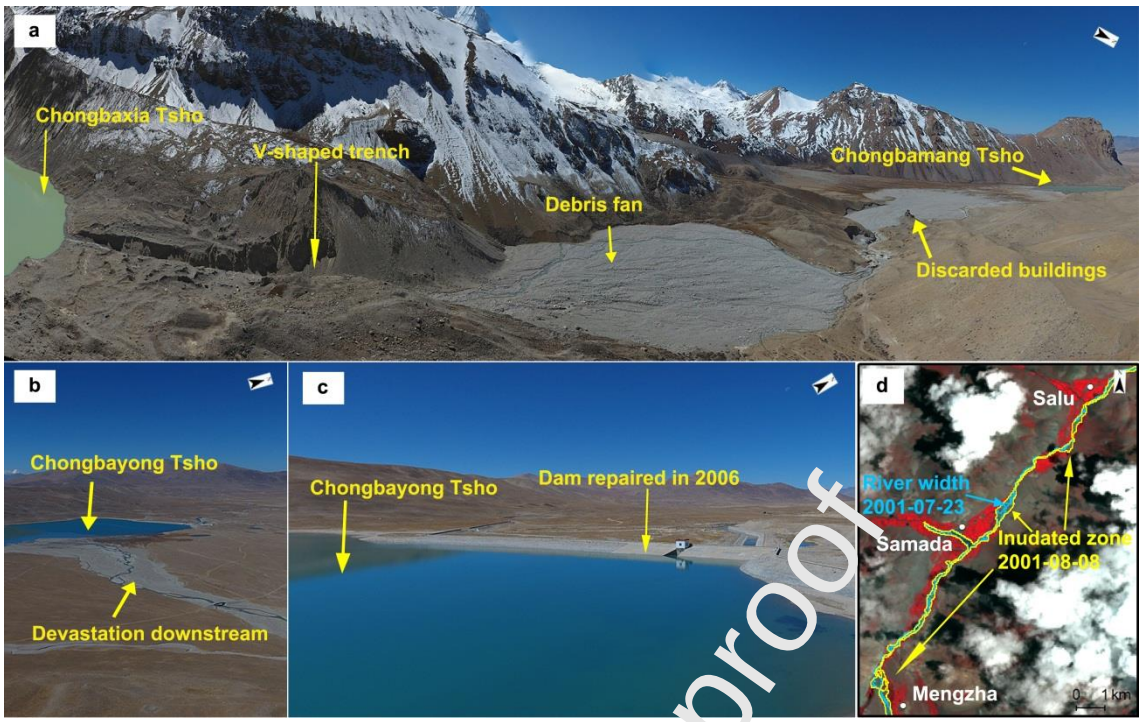

Fig. 10. Field photographs taken in 2016 showing the impacts of Chongbaxia Tsho 2001 GLOF on downstream areas (panels a-c); (d) a Landsat image dated 8 August 2001 highlighting the location of key settlements downstream of the third lake in the cascade, Chongbayong Tsho, which were affected by the GLOF.

4.4. Potential triggers for the 2001 GLOF

From an analysis of lake expansion, glacier retreat and site geomorphology from satellite observations (pre- and post-GLOF Landsat, Sentinel, and Planet imagery) and field surveys, we hypothesize that an ice avalanche into Chongbaxia Tsho was likely to be the primary GLOF trigger; there is no other obvious geomorphological evidence to suggest any other kind of substantial mass flow entering Chongbaxia Tsho from the wider catchment (Fig. 11). We find no evidence to suggest that the trigger was a rock avalanche; in the absence of a clearly identifiable source area, detailed pre- and post-GLOF bathymetric surveys would be

required to identify the remnant mass of such an event in the lake, as similarly suggested by Hubbard et al., (2005).

Between 5 February 2001 and 23 July 2001 (less than one month before the GLOF occurred), Chongbaxia Tsho expanded southeastward approximate 50 m in response to recession of its parent glacier. In doing so, the parent glacier had receded so that the terminus was located above a rock buttress at the head of the lake, where the horizontal and altitudinal difference between the parent glacier terminus and the lake surface were both ~200 m (**Fig. 11**).

We hypothesize that this vertical difference is large enough to allow a mass movement, namely an ice avalanche caused by the collapse of unstable glacier ice, to develop the momentum and impact energy required to generate a displacement or seiche wave as it entered the lake, in turn triggering moraine dam overtopping and initiate a breach.

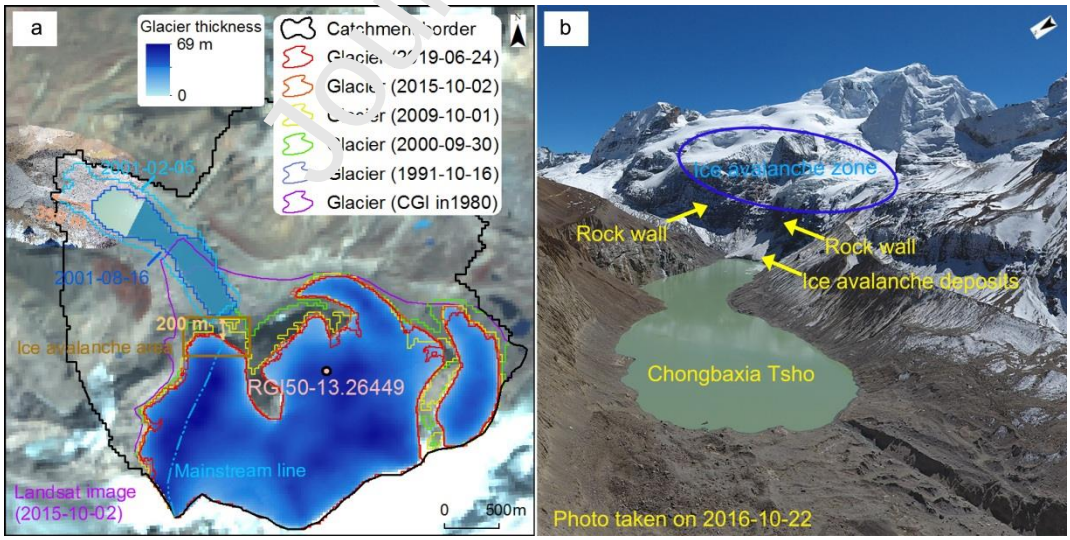

Fig. 11. Areal changes of the glacier formerly connected with Chongbaxia Tsho between 1980 and 2019, and the estimated glacier thickness in 2015 (a); field photograph showing key

geomorphological and glacial characteristics of the Chongbaxia Tsho basin, taken by the lead author (b).

5. Discussion

5.1. Contribution of climate change to GLOF hazard evolution

Climate warming drives glacier recession in the form of glacier retreat and surface downwasting, which are conducive to the development of glacial lakes (Nie et al., 2017; Jiang et al., 2018; Maurer et al., 2019). Precipitation anomalies, which can be associated with climate change, can also play an important role in triggering GLOF events (Allen et al., 2016). The mean linear warming rate for air temperature between 1987 and 2018 at the Gyangze County meteorological station, ~104 km from Chongbaxia Tsho, was 0.37 ℃ per decade (adjusted R^2 value of 0.43 and p-value of 0.01) (**Fig. 12**a). Between 1980 and 2019, the glacierized area in our study catchment reduced from 6.08 km^2 to 4.25 km^2 (**Fig. 11**a). Glacier mass loss accelerated from -0.35 m a^{-1} w.e. (meters water-equivalent) between 1975 and 2000 to -0.52 m a^{-1} w.e. per year between 2000 and 2016 (Maurer et al., 2019). In 2001, the monthly air temperature in January and February exceeded the mean values between 1987 and 2018 while air temperature from March to August was lower than the mean values (**Fig. 12**b). Annual precipitation has remained relatively stable (**Fig. 12**c) and has decreased at a rate of 3.09 mm per decade (adjusted R^2 value of 0.03 without a significant confidence interval) for the same period. In 2001, annual precipitation exceeded the historical mean by 25% (+71 mm), with the largest anomalies occurring in July (+23 mm) and August (+40 mm)

2001, producing monthly precipitation totals that both exceeded 110 mm (**Fig. 12**d). Our interpretation of these data is that whilst the short-term contribution of enhanced warming in early 2001 to the triggering of Chongbaxia Tsho GLOF event is difficult to establish, the longer-term trend of regional climate warming played a clear role in driving glacier retreat and moraine-dammed lake evolution. We further hypothesize that positive precipitation anomalies in the month preceding the GLOF, and in its month of occurrence, potentially contributed to glacier instability; elsewhere in the Himalaya, climate- and weather-driven forcing have been shown to contribute to glacier instability (Kääb et al., 2018). The final factor in the evolution (and eventual realization) of the GLOF hazard at this site was the underlying topography, which provided the conditions necessary to generate an ice avalanche with enough momentum to ultimately trigger moraine dam overtopping and eventual failure.

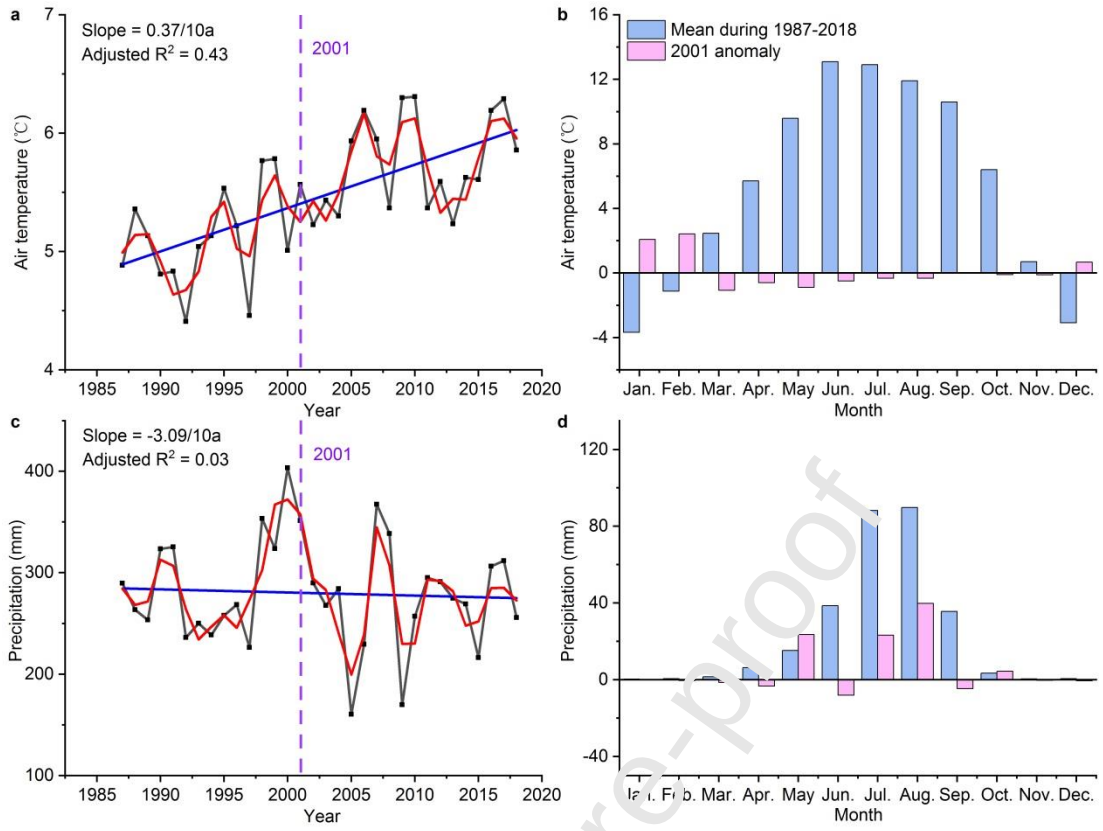

Fig. 12. Annual and monthly changes in air temperature and precipitation from the nearest meteorological station at Gyangze County between 1987 and 2018: (a) annual air temperature, (b) monthly air temperature, (c) annual precipitation and (d) monthly precipitation. The blue line addresses the linear regression and the red curve represents the 5-year moving average (a, c).

5.2. Future hazard of Chongbaxia Tsho

Further GLOFs from Chongbaxia Tsho cannot be ruled out, however the likely magnitude of future event is far lower than that in 2001. Fresh ice avalanche deposits at the base of the rock cliff are visible in Planet images from 2016 and 2019, and were confirmed as such during field investigation in 2016, implying a high frequency of low-magnitude ice

avalanching post-GLOF. The large relative volume of the parent glacier (1.6×10^8 m^3) compared to the estimated residual volume of the lake ($14.0\pm1.9 \times 10^6$ m^3; after Cook and Quincey, (2015)) suggests that, should a large-scale detachment of the parent glacier occur, the mass and momentum of such an event could displace enough water to trigger another GLOF. The large-scale detachment of two glaciers in the Aru range of western Tibet in 2016 was documented by Kääb et al. (2018), and similar events have been reported from elsewhere (Falaschi et al., 2019; Jacquemart et al., 2020). However, detailed lake bathymetry, and therefore volume, data are not currently available for Chongbaxia Tsho, and further field investigation is required in this regard so that future GLOF simulations could be parameterized as accurately as possible. Another presumption is that the existing breach in the moraine may be able to accommodate a considerable outflow discharge before further lateral erosion and vertical incision is initiated. However, there is a 53.4‰ gradient and difference (22 m) between the elevation of the distal moraine toe and the current lake level, which is a primary factor governing the maximum potential breach incision and total discharge of a future GLOF, and further field investigation is required to establish what the 'true' potential GLOF volume at the source might be. Finally, the evident buffering role of the two downstream lakes, and the improved artificial dam of Chongbayong Tsho would likely play a role in buffering the downstream impact of a future GLOF in the same way that they did for the 2001 event by attenuating the GLOF hydrograph, although the extent of this buffering is dependent on the flow characteristics of a future event.

5.3. Uncertainty and prospects

5.3.1. *Limitations and improvements in GLOF monitoring technologies*

Remote sensing has been proven to be the best way to identify or detect historical GLOFs and monitor the hazard posed by glacial lakes in remote, mountainous regions, where field access can be severely limited (Nie et al., 2018; Veh et al., 2019). It is often difficult to pinpoint the specific date of GLOFs that have occurred since the advent of satellite remote sensing primarily due to the constraints imposed by overpass revisit intervals, and the lack of high quality imagery (i.e. cloud-free, or minimal cloud coverage) for specific periods, such as those affected by the monsoon. Since 1982, Landsat sensors have a revisit interval of 16 days, Sentinel-2 can provide data at a revisit interval of 5 days since 2015, and the Planet Cubesat constellation can image the entire Earth daily (Planet Team, 2017). However, the utility of imagery acquired by the current generation of optical satellite sensors is still affected by factors such as cloud coverage, shadows cast by extreme topography, and heavy snow covers. One potential solution is to use synthetic aperture radar (SAR), which is unaffected by these constraints; SAR data acquired by the Sentinel-1 satellite has been freely available since 2014 and has been used to delineate and monitor glacial lakes (Wangchuk et al., 2019) and to classify slope processes in mountainous terrain using SAR time series data (Dini et al., 2019). These gradual improvements in the temporal resolution of high-resolution satellite imagery should allow us to ascertain the date of recent or future GLOFs with more certainty than for GLOFs that occurred a number of decades ago. When combined with the increasing availability of field- or reanalysis-derived meteorological and environmental observation networks, the synergy of these datasets should in turn allow us to develop a more robust

understanding of precise triggering events for individual GLOFs (e.g. short-lived, extreme precipitation or temperature anomalies, seismic activity).

5.3.2. Hydrodynamic modelling considerations

Our dam breach and GLOF modelling workflow did not consider mass movement-lake interactions, such as impact wave generation and propagation, and the implications for the precise mode and timescales involved in breach initiation and outflow hydrograph generation. We did not adopt more advanced, physically-based models for simulating a potential GLOF trigger (such as Mergili et al., (2017)) because we lack reliable data on the source location and precise volume of a mass movement from the parent glacier or elsewhere in the catchment. There are also no historical downstream hydrographs against which we can validate our modelled GLOF discharges. However, a lack of such data is an inherent problem when reconstructing historical GLOFs in remote areas, and ones which may be overcome with future improvements in remote sensing capability and field instrumentation.

GLOF flow processes can be very complex (Zhou et al., 2019), and flows can transform from clear water flow, to hyperconcentrated flow, to a debris flow, and these rheological transformations can occur in both space and time as the flow evolves (Worni et al., 2014; Westoby et al., 2014a). Our 2D hydrodynamic model does not account for the effects of sediment on flow rheology, or the erosion and deposition of sediment along the flow path. Models that can simulate such processes (e.g. Mergili et al., 2017; Lala et al., 2018; Vetsch et al., 2020) are more computationally intensive to run, and require site-specific information for

model parameterization which we lack, such as the grain size distribution of the flow path, and the lateral extent and depth of entrainable material (Westoby et al., 2014b; Mergili et al., 2017; Lala et al., 2018). Crucially, we also lack a high-resolution pre-GLOF DEM, which could be differenced with a post-GLOF DEM to reveal patterns of erosion and deposition that are attributable to GLOF passage, and which could be used to calibrate or validate the performance of a more advanced hydrodynamic code.

In the case of the Chongbaxia Tsho GLOF we consider that the effect of downstream sediment transport on flood propagation is perhaps more limited than for other events because of the buffering effect of the two lakes downstream. Whilst our modelling approach permits the GLOF to flow 'over' these lakes (i.e. they are not considered as true storage elements), in reality the vast majority of sediment that originated from the moraine, and was entrained from the floodplain immediately downstream of the moraine, would have been deposited either close to the moraine (for the largest size fractions), as observed during field investigation, and for other moraine-dam failures (Westoby et al., 2014b), or at the upstream limit of the second lake in the cascade, Chongbamang Tsho. However, the downstream of Chongbamang Tsho floodplain topography is laterally constrained, and our modelling results imply higher flow velocities (>15m s^{-1}) and high flow depth (>14 m) in these reaches which may have generated bed shear stresses capable of mobilizing sediment in volumes that were high enough to affect the flow rheology, although we do not quantify this.

Finally, we have shown that UAV-derived DEM products, which can be generated at low-cost, and at very high spatial resolutions, are invaluable for retrieving key site

information, and we predict that such technologies will play an increasingly important role in GLOF reconstruction and hazard assessment. Accurate pre- and post-outburst DEMs are required to estimate changes in lake level, which in turn make it possible to estimate the volume of water released by a GLOF, which can be an important input parameter for dam breach modelling.

Summary and conclusions

This study has reconstructed the hazard evolution, process and impact of a historical GLOF from Chongbaxia Tsho in the eastern Himalaya using a combination of time-series satellite imagery analysis, satellite-derived DEMs, numerical dam-breach and hydrodynamic simulation, and field observations and data collection, including deployment of a UAV to retrieve high-resolution, post-event site topography. The main conclusions arising from this work are that:

- Contrary to prior estimates, the Chongbaxia Tsho GLOF event occurred on 6 August 2001, and was most likely triggered by an ice avalanche into the lake. The lake area of Chongbaxia Tsho rapidly expanded prior to the outburst and has since remained stable.
- The GLOF released an estimated total water volume of $27.1 \pm 1.6 \times 10^6$ m^3 and achieved a peak discharge of 6625 m^3 s^{-1}. The most likely trigger for the outburst was an ice avalanche originating from the parent glacier, whose terminus had receded to atop a rock buttress some ~200 m above the lake level, providing the topographic conditions necessary to generate a mass movement with enough momentum and impact energy to produce an overtopping wave which could have initiated moraine breach development.

- Two lakes in the GLOF path, Chongbamang Tsho and Chongbayong Tsho, served a significant buffering function by attenuating the GLOF hydrograph. The latter lake is estimated to have stored ~96% of the total flood flow; the remainder was released via its artificial dam, which was damaged in the process. These lakes almost certainly reduced the downstream impacts of the GLOF and are in large part responsible for the lack of recorded fatalities associated with the outburst.
- Climate change played a crucial role in GLOF hazard development by providing the conditions necessary for sustained glacier retreat and moraine-dammed lake development. Positive precipitation anomalies in the weeks preceding the GLOF may have played an important role in determining the timing of an ice avalanche-induced triggering event, and the increasing frequency and magnitude of such anomalies as a result of climate change should be considered in future GLOF hazard assessments.
- The synergy of current and future generations of optical- and SAR-based RS observation will improve our capacity to detect GLOFs and monitor potentially dangerous glacial lakes, perhaps in a near-continuous manner. However, detailed field investigation, *in situ* hydrological and meteorological observation, and the sharing of these data play an equally important role in GLOF reconstruction and prediction.

Acknowledgements

This study was supported by the National Natural Science Foundation of China (Grant Nos. 41571104, 41971153), the Chinese Academy of Sciences "Light of West China" Program, and the CPC Sichuan Provincial Committee Organization Department Talents

Program. We acknowledge the United States Geological Survey, European Space Agency, and Planet Labs for access to satellite imagery used in this study.

References

Allen, S.K., Rastner, P., Arora, M., Huggel, C., Stoffel, M., 2016. Lake outburst and debris flow disaster at Kedarnath, June 2013: hydrometeorological triggering and topographic predisposition. Landslides, 13: 1479-1491.

Allen, S.K., Zhang, G., Wang, W., Yao, T., Bolch, T., 2019. Potentially dangerous glacial lakes across the Tibetan Plateau revealed using a large-scale automated assessment approach. Science Bulletin, 64: 435-445.

ASF DAAC, 2015. ALOS PALSAR_Radiometric_Terrain_Corrected_Hi_res; Includes Material © JAXA/METI 2007, Accessed through ASF DAAC on 26 June 2018.

Audusse, E., Bouchut, F., Bristeau, M., Klein, R., Perthame, B.T., 2004. A Fast and Stable Well-Balanced Scheme with Hydrostatic Reconstruction for Shallow Water Flows. SIAM J. Sci. Comput., 25: 2050-2065.

Biemans, H., Siderius, C., Lutz, A.F., Nepal, S., Ahmad, B., Hassan, T., von Bloh, W., Wijngaard, R.R., Wester, P., Shrestha, A.B., Immerzeel, W.W., 2019. Importance of snow and glacier meltwater for agriculture on the Indo-Gangetic Plain. Nature Sustainability, 2: 594-601.

Bohner, J., 2006. General climatic controls and topoclimatic variations in Central and High Asia. Boreas, 35: 279-295.

Bookhagen, B., Burbank, D.W., 2006. Topography, relief, and TRMM-derived rainfall variations along the Himalaya. Geophys. Res. Lett., 33: L08405.

Boulton, S.J., Stokes, M., 2018. Which DEM is best for analyzing fluvial landscape development in mountainous terrains? Geomorphology, 310: 168-187.

BP, 2019. BP Statistical Review of World Energy, London, UK.

Brun, F., Berthier, E., Wagnon, P., Kääb, A., Treichler, D., 2017. A spatially resolved estimate of High Mountain Asia glacier mass balances from 2000 to 2016. Nat. Geosci., 10: 668-673.

Byers, A.C., Rounce, D.R., Shugar, D.H., Lala, J.M., Byers, E.A., Regmi, D., 2019. A rockfall-induced glacial lake outburst flood, Upper Barun Valley, Nepal. Landslides, 16: 533-549.

Carrivick, J.L., Tweed, F.S., 2016. A global assessment of the societal impacts of glacier outburst floods. Global Planet. Change, 144: 1-16.

Chen, X.Q., Cui, P., Li, Y., Yang, Z., Qi, Y.Q., 2007. Changes in glacial lakes and glaciers of post-1986 in the Poiqu River basin, Nyalam, Xizang (Tibet). Geomorphology, 88: 273-311.

Colomina, I., Molina, P., 2014. Unmanned aerial systems for photogrammetry and remote sensing: A review. ISPRS J. Photogramm., 92: 79-97.

Cook, S.J., Quincey, D.J., 2015. Estimating the volume of Alpine glacial lakes. Earth Surf. Dynam., 3: 559-575.

Copernicus, 2019. Sentinel data (last access in 2019 at https://scihub.copernicus.eu/dhus/#/home), processed and distributed by ESA.

de Almeida, G.A.M., Bates, P., Freer, J.E., Souvignet, M., 2012. Improving the stability of a simple formulation of the shallow water equations for 2-D flood modeling. Water Resour. Res., 48: W05528.

Dini, B., Daout, S., Manconi, A., Loew, S., 2019. Classification of slope processes based on multitemporal DInSAR analyses in the Himalaya of NW Bhutan. Remote Sens. Environ., 233: 111408.

Evans, S.G., 1986. The maximum discharge of outburst floods caused by the breaching of man-made and natural dams. Can. Geotech. J., 23: 385-387.

Falaschi, D., Kääb, A., Paul, F., Tadono, T., Rivera, J.A., Lenzano, L.E., 2019. Brief communication: Collapse

of 4 Mm3 of ice from a cirque glacier in the Central Andes of Argentina. The Cryosphere, 13: 997-1004.

Farinotti, D., Huss, M., Fürst, J.J., Landmann, J., Machguth, H., Maussion, F., Pandit, A., 2019. A consensus estimate for the ice thickness distribution of all glaciers on Earth. Nat. Geosci., 12: 168-173.

Farr, T.G., Rosen, P.A., Caro, E., Crippen, R., Duren, R., Hensley, S., Kobrick, M., Paller, M., Rodriguez, E., Roth, L., Seal, D., Shaffer, S., Shimada, J., Umland, J., Werner, M., Oskin, M., Burbank, D., Alsdorf, D., 2007. The Shuttle Radar Topography Mission. Rev. Geophys., 45: RG2004.

Gao, J., Yao, T., Valérie, M., Hans, C.S., Wang, W., 2019. Collapsing glaciers threaten Asia's water supplies. Nature, 565: 19-21.

Grohmann, C.H., 2018. Evaluation of TanDEM-X DEMs on selected Brazilian sites: Comparison with SRTM, ASTER GDEM and ALOS AW3D30. Remote Sens. Environ., 212: 121-133.

Guo, W., Liu, S., Xu, J., Wu, L., Shangguan, D., Yao, X., Wei, J., Bao, W., Yu, P., Liu, Q., Jiang, Z., 2015. The second Chinese glacier inventory: data, methods and results. J. Glaciol., 61: 357-372.

Haeberli, W., 2017. Integrative modelling and managing new landscapes and environments in de-glaciating mountain ranges: An emerging trans-disciplinary research field. Forestry Research and Engineering: International Journal, 1: 1-4.

Hall, D.K., Foster, J.L., Verbyla, D.L., Klein, A.G., Benson, C.S., 1998. Assessment of snow-cover mapping accuracy in a variety of vegetation-cover densities in central Alaska. Remote Sens. Environ., 66: 129-137.

Harrison, S., Kargel, J.S., Huggel, C., Reynolds, J., Shugar, D.H., Betts, R.A., Emmer, A., Glasser, N., Haritashya, U.K., Klimeš, J., Reinhardt, L., Schaub, Y., Wiltshire, A., Regmi, D., Vilímek, V., 2018. Climate change and the global pattern of moraine-dammed glacial lake outburst floods. The Cryosphere, 12: 1195-1209.

Hennig, T., 2015. Energy, Hydropower, and Geopolitics — Northeast India and its Neighbors: A Critical

Review of the Establishment of India's Largest Hydropower Base. ASIEN, 1: 121-142.

Hubbard, B., Heald, A., Reynolds, J.M., Quincey, D., Richardson, S.D., Luyo, M.Z., Portilla, N.S., Hambrey, M.J., 2005. Impact of a rock avalanche on a moraine-dammed proglacial lake: Laguna Safuna Alta, Cordillera Blanca, Peru. Earth Surf. Proc. Land., 30: 1251-1264.

Huss, M., Bookhagen, B., Huggel, C., Jacobsen, D., Bradley, R.S., Clague, J.J., Vuille, M., Buytaert, W., Cayan, D.R., Greenwood, G., Mark, B.G., Milner, A.M., Weingartner, R., Winder, M., 2017. Toward mountains without permanent snow and ice. Earth's Future, 5: 418-435.

ICIMOD (The International Centre for Integrated Mountain Development), 2011. Glacial Lakes and Glacial Lake Outburst Floods in Nepal. ICIMOD, Kathmandu, Nepal.

Immerzeel, W.W., van Beek, L.P.H., Bierkens, M.F.P., 2010. Climate Change Will Affect the Asian Water Towers. Science, 328: 1382-1385.

Immerzeel, W.W., Pellicciotti, F., Bierkens, M.F.P., 2013. Rising river flows throughout the twenty-first century in two Himalayan glacierized watersheds. Nat. Geosci., 6: 742-745.

Jacquemart, M., Loso, M., Leopold, M., Welty, E., Berthier, E., Hansen, J.S.S., Sykes, J., Tiampo, K., 2020. What drives large-scale glacier detachments? Insights from Flat Creek glacier, St. Elias Mountains, Alaska. Geology.

Jiang, S., Nie, Y., Liu, Q., Wang, J., Liu, L., Hassan, J., Liu, X., Xu, X., 2018. Glacier Change, Supraglacial Debris Expansion and Glacial Lake Evolution in the Gyirong River Basin, Central Himalayas, between 1988 and 2015. Remote Sens.-Basel, 10: 986.

Kääb, A., Leinss, S., Gilbert, A., Bühler, Y., Gascoin, S., Evans, S.G., Bartelt, P., Berthier, E., Brun, F., Chao, W., Farinotti, D., Gimbert, F., Guo, W., Huggel, C., Kargel, J.S., Leonard, G.J., Tian, L., Treichler, D., Yao, T.,

2018. Massive collapse of two glaciers in western Tibet in 2016 after surge-like instability. Nat. Geosci., 11: 114-120.

Lala, J.M., Rounce, D.R., Mckinney, D.C., 2018. Modeling the glacial lake outburst flood process chain in the Nepal Himalaya: reassessing Imja Tsho's hazard. Hydrol. Earth Syst. Sc., 22: 3721-3737.

Liang, Q., Borthwick, A.G.L., 2009. Adaptive quadtree simulation of shallow flows with wet–dry fronts over complex topography. Comput. Fluids, 38: 221-234.

Liang, Q., 2010. Flood Simulation Using a Well-Balanced Shallow Flow Model. J. Hydraul. Eng., 136: 669-675.

Liu, C., Tong, L., Qi, S., Zhang, S., Zheng, B., 2016. Remote sensing investigation and influence factor analysis of glacier lake outburst potential in the Himalayas. Remote Sensing for Land and Resources, 28: 110-115. (in Chinese)

Maurer, J.M., Schaefer, J.M., Rupper, S., Corley, A., 2019. Acceleration of ice loss across the Himalayas over the past 40 years. Sci. Adv., 5: eaav7266

Mcfeeters, S.K., 1996. The use of the Normalized Difference Water Index (NDWI) in the delineation of open water features. Int. J. Remote Sens., 17: 1425 - 1432.

Mergili, M., Fischer, J., Krenn, J., Pudasaini, S., 2017. R.avaflow v1, an advanced open-source computational framework for the propagation and interaction of two-phase mass flows. Geosci. Model Dev., 10: 553-569.

Mergili, M., Emmer, A., Juřicová, A., Cochachin, A., Fischer, J., Huggel, C., Pudasaini, S.P., 2018. How well can we simulate complex hydro-geomorphic process chains? The 2012 multi-lake outburst flood in the Santa Cruz Valley (Cordillera Blanca, Perú). Earth Surf. Proc. Land., 43: 1373-1389.

Mool, P.K., Bajracharya, S.R., Joshi, S.P., 2001. Inventory of glaciers, glacial lakes and glacial lake outburst

floods. Monitoring and early warning systems in the Hindu Kush-Himalayan Region, Nepal, ICIMOD, Kathmandu, Nepal.

Nie, Y., Zhang, Y., Liu, L., Zhang, J., 2010. Glacial change in the vicinity of Mt. Qomolangma (Everest), central high Himalayas since 1976. J. Geogr. Sci., 20: 667-686.

Nie, Y., Sheng, Y., Liu, Q., Liu, L., Liu, S., Zhang, Y., Song, C., 2017. A regional-scale assessment of Himalayan glacial lake changes using satellite observations from 1990 to 2015. Remote Sens. Environ., 189: 1-13.

Nie, Y., Liu, Q., Wang, J., Zhang, Y., Sheng, Y., Liu, S., 2018. An inventory of historical glacial lake outburst floods in the Himalayas based on remote sensing observations and geomorphological analysis. Geomorphology, 308: 91-106.

Niipele, J.N., Chen, J., 2019. The usefulness of alos-palsar dem data for drainage extraction in semi-arid environments in The Iishana sub-basin. Journal of Hydrology: Regional Studies, 21: 57-67.

Planet Team, 2017. Planet application program interface: in space for life on Earth, San Francisco, CA. available at: https://www.planet.com.

Quincey, D.J., Lucas, R.M., Richardson, S.D., Glasser, N.F., Hambrey, M.J., Reynolds, J.M., 2005. Optical remote sensing techniques in high-mountain environments: application to glacial hazards. Prog. Phys. Geog., 29: 475-505.

RGI Consortium, 2017. Randolph Glacier Inventory – A Dataset of Global Glacier Outlines: Version 6.0: Technical Report.

Richardson, S.D., Reynolds, J.M., 2000. An overview of glacial hazards in the Himalayas. Quatern. Int., 65–66: 31-47.

Rounce, D.R., Byers, A.C., Byers, E.A., Mckinney, D.C., 2017. Brief communication: Observations of a glacier outburst flood from Lhotse Glacier, Everest area, Nepal. The Cryosphere, 11: 443-449.

Sattar, A., Goswami, A., Kulkarni, A.V., 2019. Hydrodynamic moraine-breach modeling and outburst flood routing - A hazard assessment of the South Lhonak lake, Sikkim. Sci. Total Environ., 668: 362-378.

Schwanghart, W., Worni, R., Huggel, C., Stoffel, M., Korup, O., 2016. Uncertainty in the Himalayan energy–water nexus: estimating regional exposure to glacial lake outburst floods. Environ. Res. Lett., 11: 074005.

Shean, D., 2017. High Mountain Asia 8-meter DEMs Derived from Cross-track Optical Imagery, Version 1, NASA National Snow and Ice Data Center Distributed Active Archive Center, Boulder, Colorado USA.

Sheng, Y., Song, C., Wang, J., Lyons, E.A., Knox, B.R., Cox, J.S., Gao, F., 2016. Representative lake water extent mapping at continental scales using multi-temporal Landsat-8 imagery. Remote Sens. Environ., 185: 129-141.

Stoffel, M., Wyżga, B., Marston, R.A., 2016. Floods in mountain environments: A synthesis. Geomorphology, 272: 1-9.

Terwisscha Van Scheltinga, R.C., Cocq, G., Kleinhans, M.G., Friedrich, H., 2020. Observations of dune interactions from DEMs using through-water Structure from Motion. Geomorphology, 359: 107126.

U. S. Geological Survey, 2016. Landsat—Earth observation satellites (ver. 1.2, April 2020): U.S. Geological Survey Fact Sheet 2015–3081, 4 p., https://doi.org/10.3133/fs20153081.

USGS, 2015. The Shuttle Radar Topography Mission (SRTM) Collection User Guide, Accessed through USGS website on 10 June 2019.

Vacondio, R., Dal Palù, A., Mignosa, P., 2014. GPU-enhanced Finite Volume Shallow Water solver for fast flood simulations. Environ. Modell. Softw., 57: 60-75.

Vargo, L.J., Anderson, B.M., Horgan, H.J., Mackintosh, A.N., Lorrey, A.M., Thornton, M., 2017. Using structure from motion photogrammetry to measure past glacier changes from historic aerial photographs. J. Glaciol., 63: 1105-1118.

Veh, G., Korup, O., von Specht, S., Roessner, S., Walz, A., 2019. Unchanged frequency of moraine-dammed glacial lake outburst floods in the Himalaya. Nat. Clim. Change, 9: 379-383.

Vetsch, D., Siviglia, A., Bacigaluppi, P., Bürgler, M., Caponi, F., Conde, D., Gerke, E., Kammerer, S., Koch, A., Peter, S., Vanzo, D., Vonwiller, L., Weberndorfer, M., 2020. System Manuals of BASEMENT, Version 3.0. Laboratory of Hydraulics, Glaciology and Hydrology (VAW). ETH Zurich.

Wang, J., Sheng, Y., Tong, T.S.D., 2014. Monitoring decadal lake dynamics across the Yangtze Basin downstream of Three Gorges Dam. Remote Sens. Environ., 152: 251-269.

Wang, J., Sheng, Y., Wada, Y., 2017. Little impact of the Three Gorges Dam on recent decadal lake decline across China's Yangtze Plain. Water Resour. Res., 53: 3854-3877.

Wang, W., Gao, Y., Iribarren Anacona, P., Lei, Y., Xiang, Y., Zhang, G., Li, S., Lu, A., 2018. Integrated hazard assessment of Cirenmaco glacial lake in Zhangzangbo valley, Central Himalayas. Geomorphology, 306: 292-305.

Wang, X., Liu, S., Guo, W., Xu, J., 2008. Assessment and Simulation of Glacier Lake Outburst Floods for Longbasaba and Pida Lakes, China. Mt. Res. Dev., 28: 310-317.

Wang, X., Liu, S., Zhang, J., 2019. A new look at roles of the cryosphere in sustainable development. Advances in Climate Change Research, 10: 124-131.

Wangchuk, S., Bolch, T., Zawadzki, J., 2019. Towards automated mapping and monitoring of potentially dangerous glacial lakes in Bhutan Himalaya using Sentinel-1 Synthetic Aperture Radar data. Int. J. Remote

Sens., 40: 1-26.

Wessel, B., Huber, M., Wohlfart, C., Marschalk, U., Kosmann, D., Roth, A., 2018. Accuracy assessment of the global TanDEM-X Digital Elevation Model with GPS data. ISPRS J. Photogramm., 139: 171-182.

Westoby, M.J., Brasington, J., Glasser, N.F., Hambrey, M.J., Reynolds, J.M., 2012. 'Structure-from-Motion'photogrammetry: A low-cost, effective tool for geoscience applications. Geomorphology, 179: 300-314.

Westoby, M.J., Glasser, N.F., Brasington, J., Hambrey, M.J., Quincey, D.J., Reynolds, J.M., 2014a. Modelling outburst floods from moraine-dammed glacial lakes. Earth-Sci. Rev., 134: 137-159.

Westoby, M.J., Glasser, N.F., Hambrey, M.J., Brasington, J., Reynolds, J.M., Hassan, M.A.A.M., 2014b. Reconstructing historic Glacial Lake Outburst Floods through numerical modelling and geomorphological assessment: Extreme events in the Himalaya. Earth Surf. Proc. Land., 39: 1675–1692.

Westoby, M.J., Brasington, J., Glasser, N.F., Hambrey, M.J., Reynolds, J.M., Hassan, M.A.A.M., Lowe, A., 2015. Numerical modelling of glacial lake outburst floods using physically based dam-breach models. Earth Surf. Dynam., 3: 171-199.

Wilson, R., Harrison, S., Reynolds, J., Hubbard, A., Glasser, N.F., Wündrich, O., Iribarren Anacona, P., Mao, L., Shannon, S., 2019. The 2015 Chileno Valley glacial lake outburst flood, Patagonia. Geomorphology, 332: 51-65.

Worni, R., Huggel, C., Stoffel, M., 2013. Glacial lakes in the Indian Himalayas — From an area-wide glacial lake inventory to on-site and modeling based risk assessment of critical glacial lakes. Sci. Total Environ., 468-469: S71-S84.

Worni, R., Huggel, C., Clague, J.J., Schaub, Y., Stoffel, M., 2014. Coupling glacial lake impact, dam breach,

and flood processes: A modeling perspective. Geomorphology, 224: 161-176.

Wu, W., Wang, S., 2007. One-Dimensional Modeling of Dam-Break Flow Over Movable Beds. J. Hydraul. Eng., 133: 48-58.

Wu, W., 2016. Introduction to DLBreach–A Simplified Physically-Based Dam/Levee Breach Model, Technical Report, Clarkson University, Potsdam, NY, USA.

Xu, D., Feng, Q., 1989. Dangerous glacial lake and outburst features in Xizang Himalayas. Acta Geographica Sinica, 44: 343-352. (in Chinese)

Yao, F., Wang, J., Wang, C., Crétaux, J., 2019. Constructing long-term high-frequency time series of global lake and reservoir areas using Landsat imagery. Remote Sens. Environ., 232: 111210.

Yao, T., Thompson, L., Yang, W., Yu, W.S., Gao, Y., Guo, X.J., Yang, X.X., Duan, K.Q., Zhao, H.B., Xu, B.Q., Pu, J.C., Lu, A.X., Xiang, Y., Kattel, D.B., Joswiak, D., 2012. Different glacier status with atmospheric circulations in Tibetan Plateau and surroundings. Nat. Clim. Change, 2: 663-667.

Zarfl, C., Lumsdon, A.E., Berlekamp, J., Tydecks, L., Tockner, K., 2015. A global boom in hydropower dam construction. Aquat. Sci., 77: 161-170.

Zhong, Q., Wu, W., Chen, S., Wang, M., 2016. Comparison of simplified physically based dam breach models. Nat. Hazards, 84: 1385-1418.

Zhou, G.G.D., Zhou, M., Shrestha, M.S., Song, D., Choi, C.E., Cui, K.F.E., Peng, M., Shi, Z., Zhu, X., Chen, H., 2019. Experimental investigation on the longitudinal evolution of landslide dam breaching and outburst floods. Geomorphology, 334: 29-43.

List of figure captions

Fig. 1. Location of the study area: (a) location of Nianchu River basin in the Eastern Himalaya, (b) location of Kangmar County (black line), Chongbayong River, and the study catchment (purple line), (c) Kangmar County and the location of the study site within this region. The extent of Fig. 10d is also marked. Background in (a) and (b) are ©ESRI, and background imagery in (c) is Sentinel-2 imagery acquired on 24 June, 2019.

Fig. 2. High resolution imagery and DEM data products for the study area. (a) ortho-rectified high resolution images of Planet image on 23 October, 2016 (background) and our UAV-derived orthoimage of the moraine and immediate downstream area, derived from imagery captured on 22 October 2016 and processed using SfM methods, (b) PALSAR DEM and UAV-derived DEM extent overlaid with a field-recorded GPS route, (c, d) spatial distribution of random sampling points on stable surfaces which were used to quantify elevational differences between various DEMs. Background image in (c) is a Landsat image acquired on 19 December 2000. Background topography in (d) is a SRTM DEM.

Fig. 3. Comparison of DEM elevations for random points (Fig.2c, d).

Fig. 4. Modelling-derived hydrograph at the moraine breach. The hydrograph was constructed using the 1D DL Breach model for three initial lake level scenarios based on water level decrease uncertainty

Fig. 5. Surface area changes for the three lakes in the study catchment from 1987 to 2019.

Fig. 6. Changes in the surface area of Chongbaxia Tsho moraine-dammed lake, and along the GLOF flow path, between Feb. and Aug. 2001, including the effects of the 2001 GLOF. The pre-GLOF lake extent on 5 February 2001 (yellow line) was selected as the reference for comparing the changes. Background data are Landsat imageries in standard false color composite (Bands 4, 3 and 2 in red, green and blue channels respectively). Black rectangles highlight sudden landscape modification (i.e. development of debris fans) as a result of the 2001 GLOF.

Fig. 7. Modelled flow depth of the 2001 Chongbaxia Tsho GLOF event for various time steps, specifically the points at which the GLOF reaches (a) the upstream limit of Chongbamang

Tsho, (b) the outflow of Chongbamang Tsho, (c) Chongbayong Tsho, (d) simulation end. Background is a Sentinel-2 image acquired on 24 June 2019. Also shown is the pre-GLOF extent of Chongbaxia Tsho (blue line) on February 5, 2001.

Fig. 8. Simulated flow velocity of Chongbaxia Tsho GLOF event on Aug. 6, 2001 at different time steps (see Figure 7 caption for explanation). Also shown in (d) is the location of three cross-sections (A-C) for which hydrographs are shown in Fig. 9. Background image is as per Fig. 7.

Fig. 9. Modelled GLOF discharge at three critical cross sections along the flow path (Fig. 8d), namely the moraine breach (section A), immediately upstream of the second lake in the cascade, Chongbamang Tsho (section B), and the upstream boundary of Chongbayong Tsho (section C); (b) water volume change of Chongbaxia Tsho, Chongbamang Tsho and Chongbayong Tsho during the first 10 hours of the GLOF.

Fig. 10. Field photographs taken in 2016 showing the impacts of Chongbaxia Tsho 2001 GLOF on downstream areas (panels a-c) (d) a Landsat image dated 8 August 2001 highlighting the location of key settlements downstream of the third lake in the cascade, Chongbayong Tsho, which were affected by the GLOF.

Fig. 11. (a) Areal changes of the glacier formerly connected with Chongbaxia Tsho between 1980 and 2019, and the estimated glacier thickness in 2015; (b) field photograph showing key geomorphological and glacial characteristics of the Chongbaxia Tsho basin, taken by the lead author.

Fig. 12. Annual and monthly changes in air temperature and precipitation from the nearest meteorological station at Gyangze County between 1987 and 2018: (a) annual air temperature, (b) monthly air temperature, (c) annual precipitation and (d) monthly precipitation. The blue line addresses the linear regression and the red curve represents the 5-year moving average (a, c).

Conflicts of Interest: The authors declare no conflict of interest.

Highlights

Chongbaxia Tsho GLOF occurred on 6 August 2001, undergoing a rapid lake expansion prior to outburst.

It is most likely that the event was triggered by an ice avalanche.

A total water volume of $27.1 \pm 1.6 \times 10^6$ m^3 was released, caused a severe damage to downstream.

Downstream Chongbamang Tsho and Chongbayong Tsho greatly buffered the GLOF discharge.